

Activation-Space Uncertainty Quantification for Pretrained Networks

Richard Bergna¹ Stefan Depeweg² Sergio Calvo-Ordoñez³ Jonathan Plenk³ Alvaro Cartea³
Jose Miguel Hernández-Lobato¹

Abstract

Reliable uncertainty estimates are crucial for deploying pretrained models; yet, many strong methods for quantifying uncertainty require retraining, Monte Carlo sampling, or expensive second-order computations and may alter a frozen backbone’s predictions. To address this, we introduce **Gaussian Process Activations (GAPA)**, a post-hoc method that shifts Bayesian modeling from weights to activations. GAPA replaces standard nonlinearities with Gaussian-process activations whose posterior mean *exactly* matches the original activation, preserving the backbone’s point predictions by construction while providing closed-form epistemic variances in activation space. To scale to modern architectures, we use a sparse variational inducing-point approximation over cached training activations, combined with *local k*-nearest-neighbor subset conditioning, enabling deterministic single-pass uncertainty propagation without sampling, backpropagation, or second-order information. Across regression, classification, image segmentation, and language modeling, GAPA matches or outperforms strong post-hoc baselines in calibration and out-of-distribution detection while remaining efficient at test time.

1. Introduction

Reliable uncertainty quantification (UQ) is crucial in risk-sensitive deployments, yet many effective research methods remain impractical in modern settings (Abdar et al., 2021). Weight-space Bayesian approaches (e.g., variational BNNs) often require retraining, labeled data or multi-sample evaluation, ensembles multiply compute, and Laplace-style methods rely on curvature estimates that scale poorly as models and output spaces grow (Blundell et al., 2015; MacKay, 1992; Bergna et al., 2024; Gal and Ghahramani, 2016;

¹Department of Engineering, University of Cambridge, Cambridge, UK ²Siemens AG, Munich, Germany ³Mathematical Institute and Oxford-Man Institute, University of Oxford, Oxford, UK. Correspondence to: Richard Bergna <rsb63@cam.ac.uk>.

Lakshminarayanan et al., 2017; Ritter et al., 2018; Ortega et al., 2023). The gap is most pronounced for pretrained backbones, where weights are not expected to be modified and test-time budgets favor *single-pass* inference. In this regime, a practical post-hoc method should be single-pass, prediction-preserving, epistemic, and scalable to foundation models (Table 1).

Table 1. The gap in uncertainty quantification methods.

Method	Post-hoc	Single Pass	Preserves Mean	Epistemic UQ	Foundation Ready
BNNs	✗	✗	✗	✓	✗
Ensembles	✗	✗	—	✓	✗
MC Dropout	✗	✗	✗	✓	✗
Laplace	✓	✗	✗	✓	✗
LL-Laplace	✓	✓	✗	✓	✗
Temp. Scaling	✓	✓	✗	✗	✓
GAPA (Ours)	✓	✓	✓	✓	✓

We address this by shifting uncertainty modeling from weights to *activations*. We introduce **Gaussian Process Activations (GAPA)**, a drop-in module that replaces deterministic activations with Gaussian-process activations whose *posterior mean matches the original nonlinearity*, thereby preserving the frozen backbone’s point predictions by construction while producing activation-space epistemic variances (Figure 1). For scalability, GAPA conditions on cached training activations using a sparse approximation (compression + local *k*NN conditioning), and propagates the resulting uncertainty through the network via deterministic variance-propagation rules, enabling *single-pass* predictive uncertainty. Our contributions are

- Mean-preserving post-hoc UQ:** GAPA provides epistemic uncertainty for pretrained networks while preserving point predictions.
- Scalable conditioning:** we combine induction points and local *k*-NN conditioning for practical inference at modern scales.
- Deterministic propagation:** we derive single-pass variance propagation from activation space to output space.
- Empirical validation:** across regression, classification, segmentation, and language modelling, GAPA improves calibration and OOD detection with fast inference time.

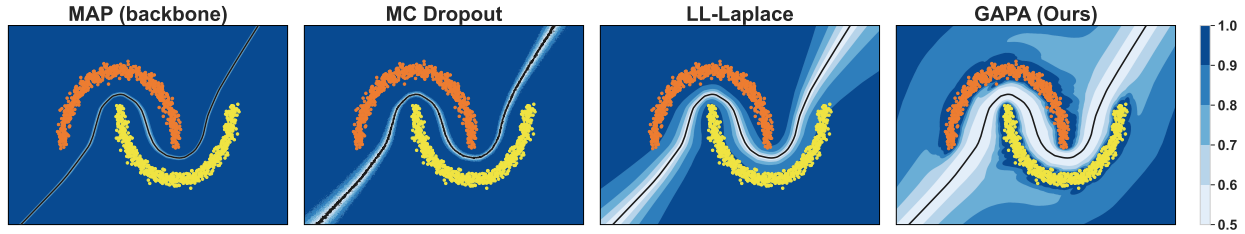


Figure 1. Comparison of uncertainty quantification methods on a toy binary classification task. **Left to right:** MAP (deterministic backbone), MC Dropout, Last-Layer Laplace, and GAPA (ours). Background shading indicates predictive confidence (darker = more confident); orange/yellow points show the two classes. **Key observation:** GAPA preserves the backbone’s decision boundary (black line) exactly while adding epistemic uncertainty that grows smoothly away from training data.

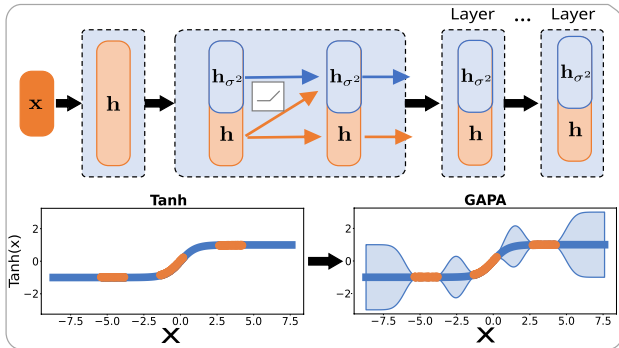


Figure 2. GAPA overview. **Top:** GAPA leaves the network’s point predictions unchanged (mean-preserving activations) while propagating an additional epistemic variance signal to the output. **Bottom left:** deterministic tanh activation; orange points denote cached training activations. **Bottom right:** GAPA-tanh, whose posterior mean matches tanh exactly; the shaded region shows ± 2 standard deviations.

2. Model Proposition

At a high level, GAPA augments a frozen neural network with activation-space uncertainty while strictly preserving its original deterministic predictions. Figure 2 provides a structural overview. In the following sections, we formalize our uncertainty perspective (Sec. 2.1), define the GP activation layer (Sec. 2.2), introduce a scalable inference mechanism (Sec. 2.3), and derive rules for single-pass variance propagation through deep architectures (Sec. 2.4).

Method pipeline. GAPA operates in two phases. **(i) Offline collection:** we run a single forward pass of a reference input training set through the pre-trained backbone and cache pre-activations at selected layers. Optionally, we compress the cache into a smaller inducing set via k -means, yielding inducing inputs that admit a variational inducing-point interpretation in the sense of Titsias (2009). **(ii) Test-time inference:** we replace deterministic activations with Gaussian-process (GP) activations that return activation-space epistemic variances. These variances are then propagated forward through the remaining frozen network using

closed-form variance propagation rules, enabling deterministic single-pass predictive uncertainty without sampling, backpropagation, or retraining, while preserving the backbone’s point predictions.

2.1. Uncertainty Modeling Perspective

We position GAPA by stating *what is random* in the predictive distribution. Let $\mathcal{D} = \{(x_n, y_n)\}_{n=1}^N$ denote the training data, and let x be a test input with corresponding output y . We denote by $f(x)$ the latent predictor (e.g., a neural network or GP) evaluated at x . Predictive uncertainty is obtained by marginalizing the latent predictor:

$$p(y | x, \mathcal{D}) = \int p(y | f(x)) p(f(x) | x, \mathcal{D}) df(x). \quad (1)$$

Weight-space uncertainty. Weight-space methods (BNNs, Laplace) parameterize $f(x) = f(x; \mathbf{w})$ and infer a posterior $\mathbf{w} \sim p(\mathbf{w} | \mathcal{D})$, inducing epistemic uncertainty via variability across plausible weights.

Activation-space uncertainty (GAPA). GAPA keeps the frozen weights deterministic and instead places epistemic uncertainty on the hidden-layer *activation* (e.g., ReLU outputs). For a chosen layer ℓ , write

$$f(x) = h_\ell(\phi(\mathbf{z}_\ell(x))),$$

where $\mathbf{z}_\ell(x)$ are layer- ℓ pre-activations, ϕ is an element-wise nonlinearity, and $h_\ell(\cdot)$ denotes the remaining frozen network. We replace ϕ with a GP activation \mathbf{g}_ℓ such that its posterior mean matches the original activation, $\mu_\ell(\mathbf{z}) = \phi(\mathbf{z})$ (Sec. 2.2), thereby preserving the backbone point prediction exactly. Let $\mathbf{a}_\ell := \mathbf{g}_\ell(\mathbf{z}_\ell(x))$ be the resulting random activation. Then

$$p(y | x, \mathcal{D}) = \int p(y | h_\ell(\mathbf{a}_\ell)) p(\mathbf{a}_\ell | \mathbf{z}_\ell(x), \mathcal{D}) d\mathbf{a}_\ell. \quad (2)$$

Uncertainty grows as test-time pre-activations move away from regions supported by the training data.

2.2. Gaussian Process Activation Function

We define the core GAPA module: a drop-in replacement for a deterministic activation that (i) preserves the frozen backbone’s point predictions exactly and (ii) returns a distance-aware epistemic variance in activation space.

Setup. Consider a frozen network and layer ℓ of width d_ℓ . Let

$$\mathbf{z}_\ell = \mathbf{W}_\ell \mathbf{h}_{\ell-1} + \mathbf{b}_\ell \in \mathbb{R}^{d_\ell}, \quad \mathbf{h}_\ell = \phi(\mathbf{z}_\ell),$$

where $\phi(\mathbf{z}) = (\phi(z_1), \dots, \phi(z_{d_\ell}))^\top$ is an element-wise nonlinearity (e.g. ReLU).

GP activation. GAPA replaces the deterministic activation $\phi(\cdot)$ with a vector-valued Gaussian process (GP)

$$\mathbf{g}_\ell(\cdot) : \mathbb{R}^{d_\ell} \rightarrow \mathbb{R}^{d_\ell}, \quad \mathbf{g}_\ell(\cdot) \sim \mathcal{GP}(\mathbf{m}_\ell(\cdot), \mathbf{K}_\ell(\cdot, \cdot)).$$

For any input \mathbf{z} , this GP induces a *Gaussian marginal distribution* over the activation vector

$$\mathbf{a}_\ell := \mathbf{g}_\ell(\mathbf{z}),$$

with posterior mean $\boldsymbol{\mu}_\ell(\mathbf{z})$ and covariance $\mathbf{K}_\ell(\mathbf{z}, \mathbf{z})$.

For scalability, we use a diagonal output kernel,

$$\mathbf{K}_\ell(\mathbf{z}, \mathbf{z}') = \text{diag}(k_{\ell,1}(\mathbf{z}, \mathbf{z}'), \dots, k_{\ell,d_\ell}(\mathbf{z}, \mathbf{z}')),$$

which is equivalent to modeling each activation dimension as an independent scalar GP. Importantly, GAPA never samples from these distributions: all uncertainty is propagated analytically via closed-form moment propagation.

Data collation for the GP. We run a single forward pass of the backbone’s training data and cache the resulting pre-activations

$$\tilde{\mathbf{Z}}_\ell = \{\tilde{\mathbf{z}}_\ell^{(m)}\}_{m=1}^M, \quad \tilde{\mathbf{z}}_\ell^{(m)} \in \mathbb{R}^{d_\ell}.$$

At each cached input we form *noiseless pseudo-observations* by evaluating the original activation,

$$\tilde{\mathbf{y}}_\ell^{(m)} = \phi(\tilde{\mathbf{z}}_\ell^{(m)}) \in \mathbb{R}^{d_\ell}, \quad m = 1, \dots, M,$$

and collect them as $\tilde{\mathbf{Y}}_\ell \in \mathbb{R}^{M \times d_\ell}$. We condition the GP on the dataset

$$\mathcal{D}_\ell = \{(\tilde{\mathbf{z}}_\ell^{(m)}, \tilde{\mathbf{y}}_\ell^{(m)})\}_{m=1}^M,$$

using a small jitter/noise term σ_n^2 for numerical stability.

Mean preservation. We choose the GP prior mean to match the original activation,

$$\mathbf{m}_\ell(\mathbf{z}) = \phi(\mathbf{z}).$$

Under standard GP regression, the posterior mean at \mathbf{z}_ℓ^* can be written as

$$\boldsymbol{\mu}_\ell(\mathbf{z}_\ell^*) = \mathbf{m}_\ell(\mathbf{z}_\ell^*) + \mathbf{A}_\ell(\mathbf{z}_\ell^*) \underbrace{(\tilde{\mathbf{Y}}_\ell - \mathbf{m}_\ell(\tilde{\mathbf{Z}}_\ell))}_{=0},$$

where $\mathbf{A}_\ell(\mathbf{z}_\ell^*) = \mathbf{K}_\ell(\mathbf{z}_\ell^*, \tilde{\mathbf{Z}}_\ell) (\mathbf{K}_\ell(\tilde{\mathbf{Z}}_\ell, \tilde{\mathbf{Z}}_\ell) + \sigma_n^2 \mathbf{I})^{-1}$. Since $\tilde{\mathbf{Y}}_\ell = \phi(\tilde{\mathbf{Z}}_\ell) = \mathbf{m}_\ell(\tilde{\mathbf{Z}}_\ell)$ by construction, the residual term is identically zero and hence

$$\boldsymbol{\mu}_\ell(\mathbf{z}_\ell^*) = \mathbf{m}_\ell(\mathbf{z}_\ell^*) = \phi(\mathbf{z}_\ell^*) \quad \text{for all } \mathbf{z}_\ell^*.$$

Therefore, the *GAPA activation* has posterior mean equal to the original activation function. Substituting $\mathbf{h}_\ell = \mathbf{g}_\ell(\mathbf{z}_\ell)$ into a frozen network preserves the backbone’s point predictions exactly. The remaining posterior covariance of the GP activation, which quantifies epistemic uncertainty in activation space, is specified next.

Posterior covariance. While the posterior mean is unchanged, the posterior covariance is non-zero and diagonal. For each neuron i ,

$$[\boldsymbol{\Sigma}_\ell(\mathbf{z}_\ell^*)]_{ii} = k_{\ell,i}(\mathbf{z}_\ell^*, \mathbf{z}_\ell^*) - \left(\mathbf{k}_{\ell,i}(\mathbf{z}_\ell^*)^\top (\mathbf{K}_{\ell,i} + \sigma_n^2 \mathbf{I})^{-1} \mathbf{k}_{\ell,i}(\mathbf{z}_\ell^*) \right),$$

where $[\mathbf{K}_{\ell,i}]_{mn} = k_{\ell,i}(\tilde{\mathbf{z}}_\ell^{(m)}, \tilde{\mathbf{z}}_\ell^{(n)})$ and $[\mathbf{k}_{\ell,i}(\mathbf{z}_\ell^*)]_m = k_{\ell,i}(\mathbf{z}_\ell^*, \tilde{\mathbf{z}}_\ell^{(m)})$. Collecting all neuron-wise variances yields the layer covariance

$$\boldsymbol{\Sigma}_\ell(\mathbf{z}_\ell^*) = \text{diag}([\boldsymbol{\Sigma}_\ell(\mathbf{z}_\ell^*)]_{11}, \dots, [\boldsymbol{\Sigma}_\ell(\mathbf{z}_\ell^*)]_{d_\ell d_\ell}). \quad (3)$$

The resulting layer covariance satisfies $\boldsymbol{\Sigma}_\ell(\mathbf{z}_\ell^*) \in \mathbb{R}^{d_\ell \times d_\ell}$ and captures neuron-wise uncertainty that increases as \mathbf{z}_ℓ^* departs from the cached pre-activations.

Why diagonal covariance? We model neurons as conditionally independent (i.e., a diagonal output covariance) for tractability. A full multi-output covariance would require storing and propagating dense $d_\ell \times d_\ell$ matrices, which is prohibitive in memory and compute for modern wide networks. The diagonal approximation is standard in scalable Bayesian models and is sufficient in our setting to capture activation-level epistemic uncertainty, as evidenced by our strong empirical results (Sec. 3).

2.3. Local Inducing-Point Approximation

At layer ℓ , GAPA conditions d_ℓ independent scalar GPs on a cache of N_ℓ pre-activations $\tilde{\mathbf{Z}}_\ell \in \mathbb{R}^{N_\ell \times d_\ell}$ obtained from a single offline forward pass of the backbone’s training data (or a subset thereof) through the frozen network. Even with

a diagonal output kernel, exact GP conditioning in Eq. (3) requires solving an $N_\ell \times N_\ell$ linear system per neuron, yielding $\mathcal{O}(d_\ell N_\ell^3)$ time and $\mathcal{O}(d_\ell N_\ell^2)$ memory, which is prohibitive for modern networks. We therefore use a two-stage approximation: (i) an *offline* global inducing set that compresses the cache, and (ii) *test-time local* conditioning on the K nearest inducing points to each query pre-activation.

Stage 1: Inducing-point construction (offline). We construct inducing inputs $\mathbf{Z}_\ell \in \mathbb{R}^{M_\ell \times d_\ell}$ with $M_\ell \ll N_\ell$ by running k -means on the cached pre-activations $\tilde{\mathbf{Z}}_\ell$ and taking the M_ℓ centroids. These inducing points provide a compressed representation of the training-data activation cache used for scalable GP inference. A formal connection between this procedure and variational inducing-point GPs is provided in Appendix B, and Appendix M.2 studies sensitivity to the number of inducing points.

Stage 2: Local K -nearest-neighbour conditioning (test time). At test time, using all M_ℓ inducing points would require an $M_\ell \times M_\ell$ solve per query, which is still expensive. We therefore adopt a local GP approximation (Gramacy and Apley, 2015): for each query pre-activation $\mathbf{z}_\ell^* \in \mathbb{R}^{d_\ell}$, we form a small local subset of inducing inputs by K -nearest neighbours in activation space.

Concretely, let $\mathcal{N}_K(\mathbf{z}_\ell^*) \subseteq \{1, \dots, M_\ell\}$ denote the indices of the K nearest inducing points to \mathbf{z}_ℓ^* under Euclidean distance, and define

$$\mathbf{Z}_{\ell,K}(\mathbf{z}_\ell^*) = \mathbf{Z}_\ell^{\mathcal{N}_K(\mathbf{z}_\ell^*)} \in \mathbb{R}^{K \times d_\ell},$$

where $\mathbf{Z}_\ell^{\mathcal{N}_K(\cdot)}$ denotes the submatrix formed by selecting the corresponding rows of \mathbf{Z}_ℓ . Neighbour retrieval is performed using FAISS (Douze et al., 2025) with approximate nearest-neighbour search, yielding sublinear query time in practice. Appendix M.5 further studies sensitivity to K .

Approximate posterior covariance. Given the local inducing inputs $\mathbf{Z}_{\ell,K}(\mathbf{z}_\ell^*) \in \mathbb{R}^{K \times d_\ell}$, we approximate the posterior variance of neuron $i \in \{1, \dots, d_\ell\}$ by applying the standard GP conditional-variance formula restricted to this local subset:

$$\begin{aligned} \sigma_{\ell,i}^2(\mathbf{z}_\ell^*) &\approx k_{\ell,i}(\mathbf{z}_\ell^*, \mathbf{z}_\ell^*) \\ &\quad - \mathbf{k}_{\ell,i}(\mathbf{z}_\ell^*)^\top (\mathbf{K}_{\ell,i} + \sigma_n^2 \mathbf{I})^{-1} \mathbf{k}_{\ell,i}(\mathbf{z}_\ell^*), \end{aligned} \quad (4)$$

where σ_n^2 is a small jitter term for numerical stability. Let $\{\mathbf{z}_{\ell,K}^{(m)}\}_{m=1}^K$ denote the rows of $\mathbf{Z}_{\ell,K}(\mathbf{z}_\ell^*)$. Then the $K \times K$ kernel matrix and K -vector are defined as

$$[\mathbf{K}_{\ell,i}]_{mn} = k_{\ell,i}(\mathbf{z}_{\ell,K}^{(m)}, \mathbf{z}_{\ell,K}^{(n)}), [\mathbf{k}_{\ell,i}(\mathbf{z}_\ell^*)]_m = k_{\ell,i}(\mathbf{z}_\ell^*, \mathbf{z}_{\ell,K}^{(m)}).$$

Collecting neuron-wise variances yields the diagonal layer covariance

$$\Sigma_\ell(\mathbf{z}_\ell^*) = \text{diag}(\sigma_{\ell,1}^2(\mathbf{z}_\ell^*), \dots, \sigma_{\ell,d_\ell}^2(\mathbf{z}_\ell^*)) \in \mathbb{R}^{d_\ell \times d_\ell}.$$

Table 2. Computational complexity per layer ℓ . Exact GP refers to conditioning on all N_ℓ cached activations. $I_{k\text{-means}}$ denotes the number of k -means iterations.

Operation	Exact GP	GAPA (Ours)
Preprocessing	$\mathcal{O}(N_\ell^3)$	$\mathcal{O}(N_\ell I_{k\text{-means}}) + \mathcal{O}(M_\ell \log M_\ell)$
Inference (per query)	$\mathcal{O}(N_\ell^2)$	$\mathcal{O}(\log(M_\ell)) + \mathcal{O}(K^3)$
Memory	$\mathcal{O}(N_\ell^2)$	$\mathcal{O}(M_\ell)$

Conservative uncertainty (monotonicity). Intuitively, conditioning a GP on fewer points cannot reduce posterior uncertainty. Fix kernel hyperparameters and observation noise $\sigma_n^2 > 0$, and let $A \subseteq C$ be two conditioning sets. Then for any test input \mathbf{z}^* ,

$$\text{Var}(f(\mathbf{z}^*) \mid \mathcal{D}_A) \geq \text{Var}(f(\mathbf{z}^*) \mid \mathcal{D}_C).$$

Consequently, conditioning on the local subset $\mathbf{Z}_{\ell,K}(\mathbf{z}_\ell^*) \subseteq \mathbf{Z}_\ell$ cannot underestimate epistemic uncertainty relative to using the full inducing set. A formal statement and proof are provided in Appendix A; we additionally ablate sensitivity to K in Appendix M.5.

Computational complexity. Offline preprocessing comprises caching $\tilde{\mathbf{Z}}_\ell$ (one forward pass), constructing \mathbf{Z}_ℓ via k -means, and building a FAISS index over \mathbf{Z}_ℓ , where typically $K \ll M_\ell \ll N_\ell$. At test time, each query requires (i) neighbour search in $\mathcal{O}(\log M_\ell)$ and (ii) solving a $K \times K$ system in Eq. (4). With fixed K (we use $K = 50$), the per-query linear algebra is constant-size and the dominant dependence on the inducing set size is $\mathcal{O}(\log M_\ell)$; memory is linear in M_ℓ . See Table 2 for a summary.

2.4. Variance Propagation Through the Network

Gaussian flow intuition. Once we replace deterministic activations with GAPA modules, the forward pass no longer carries only a point value. Instead, at any layer we track a *Gaussian summary* of the hidden state: a mean vector and a diagonal covariance matrix $\Sigma_{\mathbf{h}}$. Concretely, each GAPA layer maps a (possibly uncertain) pre-activation input to a Gaussian output, so uncertainty can be *propagated forward* through the remaining frozen layers. Specialized rules for architectures such as self-attention and RMSNorm are provided in Appendix K.

Notation. We denote by $\mu_{\mathbf{h}}$ the mean of a vector-valued random variable \mathbf{h} and by $\Sigma_{\mathbf{h}}$ its covariance matrix. We write the *variance vector* $\mathbf{v}_{\mathbf{h}} := \text{diag}(\Sigma_{\mathbf{h}})$, whose entries are $[\mathbf{v}_{\mathbf{h}}]_i = \text{Var}(h_i)$. For vectors \mathbf{a}, \mathbf{b} of the same size, $\mathbf{a} \odot \mathbf{b}$ denotes the *Hadamard* (element-wise) product, and $\mathbf{a}^{\odot 2} := \mathbf{a} \odot \mathbf{a}$.

(i) Linear layers. Consider a linear transformation $\mathbf{z} = \mathbf{W}\mathbf{h} + \mathbf{b}$ where \mathbf{h} has diagonal covariance. Under the diag-

onal approximation, the output variance remains diagonal and the variance vector propagates as

$$\mathbf{v}_z = (\mathbf{W} \odot \mathbf{W}) \mathbf{v}_h. \quad (5)$$

Intuitively, each output coordinate $z_i = \sum_j W_{ij} h_j$ is a weighted sum of independent components, so its variance is the sum of squared weights times input variances.

(ii) Element-wise nonlinearities (delta method). We use first-order moment propagation (delta method): means follow the deterministic forward pass, while variances are updated by local linearization. Let $y = g(z)$ where $z \sim \mathcal{N}(\mu, \sigma^2)$ and g is a scalar nonlinearity (e.g., ReLU, tanh). We linearize around μ :

$$g(z) \approx g(\mu) + g'(\mu)(z - \mu).$$

This gives the standard delta-method moments:

$$\mathbb{E}[y] \approx g(\mu), \quad \text{Var}(y) \approx (g'(\mu))^2 \sigma^2. \quad (6)$$

Applied element-wise to vectors $\mathbf{y} = g(\mathbf{z})$ with diagonal variances, yields

$$\boldsymbol{\mu}_y = g(\boldsymbol{\mu}_z), \quad \mathbf{v}_y \approx (g'(\boldsymbol{\mu}_z))^{\odot 2} \odot \mathbf{v}_z. \quad (7)$$

Intuitively, a nonlinearity either amplifies or attenuates uncertainty depending on its local slope.

(iii) Stacking GAPA layers (noisy-input correction).

When we place multiple GAPA layers in a network, the input to a downstream GAPA layer is no longer a point \mathbf{z}^ℓ but a *distribution* (summarized as a Gaussian with mean $\boldsymbol{\mu}_z$ and variance vector \mathbf{v}_z). Standard GP conditioning assumes a deterministic test input; here the test-time input is itself uncertain. Intuitively, even if the GP were evaluated at the same mean location, uncertainty in the input location induces additional variability in the output whenever the GP mean changes with \mathbf{z} . Following the noisy-input GP (NIGP) approximation (McHutchon and Rasmussen, 2011), we capture this effect by adding a first-order correction term.

Concretely, for neuron i at layer ℓ , we evaluate the local inducing-point posterior variance at the mean input and add the NIGP correction

$$\sigma_{\ell,i}^2(\mathbf{z}^\ell) \approx \underbrace{\sigma_{\text{epi},\ell,i}^2(\boldsymbol{\mu}_z)}_{\text{epistemic}} + \underbrace{\lambda_{\ell,i}(\boldsymbol{\mu}_z)}_{\text{input uncertainty}} + \underbrace{\sigma_{y,i}^2}_{\text{aleatoric}},$$

where $\sigma_{\text{epi},\ell,i}^2(\boldsymbol{\mu}_z)$ is the local GP variance from Eq. (4) computed using the K -NN subset selected at $\boldsymbol{\mu}_z$, and

$$\lambda_{\ell,i}(\boldsymbol{\mu}_z) = (\nabla_{\mathbf{z}^\ell} \mu_{\ell,i}(\boldsymbol{\mu}_z))^\top \text{diag}(\mathbf{v}_z) (\nabla_{\mathbf{z}^\ell} \mu_{\ell,i}(\boldsymbol{\mu}_z))$$

is the NIGP correction induced by input uncertainty. In our mean-preserving element-wise setting $\mu_{\ell,i}(\mathbf{z}) = \phi_\ell(z_i)$, this simplifies to $\lambda_{\ell,i}(\boldsymbol{\mu}_z) = (\phi'_\ell(\mu_{z,i}))^2 v_{z,i}$. We set $\sigma_{y,i}^2 = 0$ for classification; for regression we add a learned heteroscedastic noise head (Sec. 2.5).

2.5. Hyperparameter Strategy

A key design choice in GAPA is to *fix* GP hyperparameters rather than optimize them.

Empirical (post-hoc) hyperparameters. GAPA is designed as a *post-hoc* module for pretrained neural networks: after standard training, we attach GAPA using only one forward pass on the backbone’s input training data (or a subset thereof) to cache activations, without any additional back-propagation, fine-tuning or labels. Accordingly, we set GP hyperparameters *once* from simple empirical statistics of the cached pre-activations. Because hyperparameters are estimated from activation statistics rather than a task-specific objective, the method is task-agnostic: the same procedure applies across settings (e.g., regression, classification, token prediction, and segmentation). Caching is a one-off offline step, and test-time inference remains unchanged thereafter. Details of the empirical hyperparameter construction are given in Appendix G.1.

We use an RBF kernel $k_{\ell,i}(\mathbf{z}, \mathbf{z}') = c_i^2 \exp(-\|\mathbf{z} - \mathbf{z}'\|^2 / (2\ell_i^2))$, with (c_i^2, ℓ_i) set from cached activation statistics and a small jitter. Details are given in Appendix G.1, with downstream likelihoods for classification and regression described in Appendix I and Appendix G.2.

3. Results

We evaluate GAPA as a *post-hoc* uncertainty module for *frozen* pretrained backbones across regression (Sec. 3.1), classification (Sec. 3.2), image segmentation (Appendix Sec. E), and language modeling (Sec. F). Ablations on layer placement, inducing-set size M , local subset size K , and uncertainty-score choices are provided in Appendix M.

3.1. Regression

Setup and baselines. We evaluate on three regression benchmarks using the original train/test splits: YEAR Prediction MSD, Airline (Hensman et al., 2013), and Taxi (Salimbeni and Deisenroth, 2017). We compare against: **MAP** (backbone model), **Dropout** (MC Dropout with multiple stochastic forward passes; (Gal and Ghahramani, 2016)), **Ensemble** (independently trained models; (Lakshminarayanan et al., 2017)), and post-hoc last-layer Bayesian baselines (**LLA** variants, **ELLA**, **VaLLA**; (Ortega et al., 2023)).

Metrics. Performance is evaluated using Negative Log-Likelihood (NLL), Continuous Ranked Probability Score (CRPS), and the Centered Quantile Metric (CQM), with definitions in Appendix J.1.

Table 3 shows a consistent pattern across all regression benchmarks. GAPA achieves the best NLL on all three

Table 3. Results on regression datasets. Best values are in purple, and second-best in teal. An asterisk (*) indicates a last-layer LLA variant. Results are averages over 5 random seeds; standard deviations ($< 10^{-3}$ in all cases) are omitted for brevity. The full table with stds can be found in Table 7 in the Appendix.

Model	Airline			Year			Taxi		
	NLL	CRPS	CQM	NLL	CRPS	CQM	NLL	CRPS	CQM
MAP	5.121	18.695	0.148	3.673	5.023	0.134	3.775	3.755	0.211
LLA Diag	5.125	18.648	0.143	3.647	4.917	0.088	3.722	3.990	0.257
LLA KFAC	5.127	18.631	0.142	3.648	4.915	0.086	3.706	3.986	0.256
LLA*	5.127	18.631	0.141	3.648	4.915	0.086	3.726	3.985	0.256
LLA*KFAC	5.127	18.631	0.141	3.648	4.914	0.086	3.726	3.985	0.256
ELLA	5.388	21.671	0.413	4.020	6.049	0.424	3.885	3.680	0.219
VaLLA100	4.963	18.814	0.099	3.515	5.004	0.047	3.235	3.999	0.149
VaLLA200	4.965	18.788	0.098	3.485	4.970	0.041	3.232	3.979	0.142
Dropout	5.102	19.066	0.938	3.689	5.128	0.939	3.849	4.592	0.951
Ensemble	5.053	18.205	0.933	3.639	4.833	0.938	3.631	3.384	0.961
GAPA	4.946	18.068	0.103	3.470	4.663	0.014	3.112	4.035	0.104

datasets, indicating the strongest overall fit of the predictive distribution. Moreover, GAPA attains the best CQM overall, demonstrating consistently well-calibrated predictive quantiles. CRPS follows the same trend on Airline and Year, with a small degradation on Taxi, where ELLA perform best.

3.2. Classification

We now evaluate classification performance in terms of accuracy and calibration, and assess OOD detection via AUC using predictive entropy and BALD. Metric definitions are provided in Appendix J.2.

Baselines. We compare against (i) the deterministic backbone (MAP); (ii) sampling-based baselines requiring multiple forward passes or multiple trainings (MC Dropout (Gal and Ghahramani, 2016), Deep Ensembles (Lakshminarayanan et al., 2017)); (iii) post-hoc last-layer Bayesian baselines that Bayesianize only the head (LLA/ELLA/VaLLA; (Ortega et al., 2023)); and (iv) distance-/feature-based alternatives including SNGP (Liu et al., 2020), MF-VI (Blundell et al., 2015), and a subset GP baseline based on the GP interpretation of local linearization. We also report linear probing (Alain and Bengio, 2016) as a lightweight head-only baseline, and DDU (Mukhoti et al., 2023) as a post-hoc feature-density uncertainty estimator.

MNIST / FMNIST (MLP). Following Ortega et al. (2023), we train a 2-layer MLP with 200 hidden units and tanh activations on MNIST (LeCun et al., 2002) and Fashion-MNIST (Xiao et al., 2017). We evaluate OOD detection by swapping datasets: Fashion-MNIST is treated as OOD for MNIST (MNIST→FMNIST) and MNIST as OOD for Fashion-MNIST (FMNIST→MNIST), reporting AUROC based on predictive entropy and BALD-OOD (Table 4). Since GAPA is mean-preserving, it leaves the back-

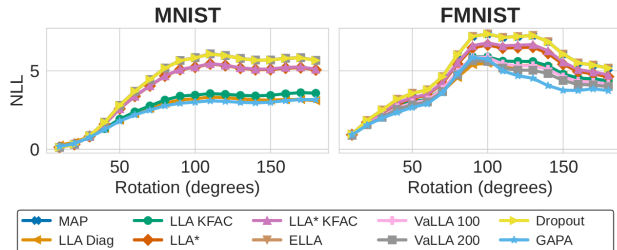


Figure 3. Predictive NLL under rotation corruption for MNIST (left panel) and FMNIST (right panel); lower is better. Results are averaged over 5 random seeds.

bone’s point predictions unchanged, and therefore matches the MAP classifier in accuracy by construction. GAPA achieves the best BALD AUROC in both directions and the best predictive-entropy AUROC on FMNIST→MNIST, while remaining competitive on MNIST→FMNIST. Moreover, GAPA enables deterministic single-pass inference with near-MAP runtime (2.05s test time), yielding substantial speedups over Monte Carlo and curvature-based baselines.

Robustness under distribution shift. We evaluate robustness by rotating the *test* images by increasing angles and plotting predictive NLL for MNIST and FMNIST as shown in Figure 3. As rotation increases and inputs move further from the training distribution, GAPA maintains competitive NLL under shifts and achieves lower NLL than most baselines for large rotations, while appropriately increasing uncertainty. This indicates robust and well-calibrated behaviour, with the model correctly identifying heavily rotated inputs as out-of-distribution.

CIFAR-10 (pretrained ResNets). We evaluate CIFAR-10 with pretrained ResNet-20/32/44/56 backbones (He et al., 2016) and use SVHN as the OOD dataset. Here the central question is the *robustness–efficiency trade-off*: many strong OOD baselines are prohibitively expensive at inference, while fast methods often sacrifice OOD detection. On representative ResNet-44/56 backbones (Table 5), GAPA attains strong OOD AUROC (0.931/0.953) with low test-time cost (2.85s/3.30s), compared to the most accurate-but-slow baselines such as VaLLA and GP-subset (test costs in the 10^2 – 10^3 s range). Figure 4 makes this explicit, GAPA lies on, or very close to, the Pareto frontier, offering one of the best OOD–inference cost trade-offs for all ResNet-20/32/44/56.

3.3. Language models

We attach GAPA post hoc to LLaMA-3.2-3B (hidden size 3072). For each chosen transformer block (we report layer indices), we log ~ 12 M pre-activations on WikiText-103 (training split) at sequence length $L = 96$ and build a nearest-neighbor cache for uncertainty propagation. We use KMeans as preprocessing step, in Appendix F we also

Table 4. Classification performance and runtime on MNIST and Fashion-MNIST. Accuracy (ACC), negative log-likelihood (NLL), expected calibration error (ECE), OOD detection, and BALD are reported. Best results are shown in purple and second-best in teal. All results are averaged over 5 random seeds; standard deviations ($< 10^{-3}$) are omitted. Training and test times are wall-clock seconds ($K = 10^3$). The full table with standard deviations is provided in Table 7 in the Appendix.

Model	MNIST							FMNIST						
	Metrics					Time (s)		Metrics					Time (s)	
	ACC	NLL	ECE	OOD	BALD	Train	Test	ACC	NLL	ECE	OOD	BALD	Train	Test
MAP (backbone)	0.978	0.068	0.005	0.919	0.919	—	1.24	0.859	0.392	0.007	0.846	0.821	—	1.20
LLA Diag	0.976	0.177	0.105	0.932	0.941	2.34K	2.39	0.856	0.421	0.057	0.872	0.873	2.34K	2.22
LLA KFAC	0.978	0.102	0.042	0.971	0.971	130.0	2.85	0.858	0.395	0.020	0.909	0.970	129.9	2.84
LLA*	0.978	0.070	0.009	0.924	0.924	42.0	4.6	0.859	0.395	0.019	0.850	0.716	42.0	4.7
LLA* KFAC	0.979	0.070	0.009	0.923	0.928	31.2	17.6	0.859	0.394	0.017	0.849	0.717	31.2	17.4
ELLA	0.978	0.068	0.005	0.919	0.912	821.8	148.7	0.859	0.392	0.007	0.846	0.765	827.1	149.9
VaLLA 100	0.978	0.068	0.005	0.919	0.934	2.19K	16.4	0.865	0.382	0.019	0.925	0.963	495.1	16.4
VaLLA 200	0.978	0.068	0.005	0.919	0.934	3.43K	18.3	0.867	0.378	0.020	0.937	0.970	767.7	19.3
Linear Probing	0.977	0.117	0.015	0.884	0.883	2.78K	3.6	0.858	0.395	0.048	0.785	0.776	2.64K	3.8
GPP	0.978	1.648	0.784	0.934	0.904	5.79K	23.5K	0.857	1.716	0.692	0.867	0.962	5.57K	2.27K
Dropout	0.978	0.072	0.009	0.923	0.944	—	4.3	0.858	0.393	0.009	0.850	0.911	—	4.3
Ensemble	0.979	0.069	0.038	0.936	0.962	—	11.9	0.859	0.373	0.041	0.863	0.938	—	11.9
DDU (est.)	0.978	0.068	0.005	0.921	0.919	202.4	8.2	0.859	0.392	0.007	0.876	0.983	202.3	8.2
GAPA-Diag	0.978	0.073	0.016	0.963	0.976	91.9	2.05	0.859	0.390	0.009	0.941	0.993	92.1	2.05
GAPA-Full	0.978	0.072	0.013	0.969	0.983	96.1	8.92	0.859	0.388	0.009	0.990	0.997	96.1	8.91

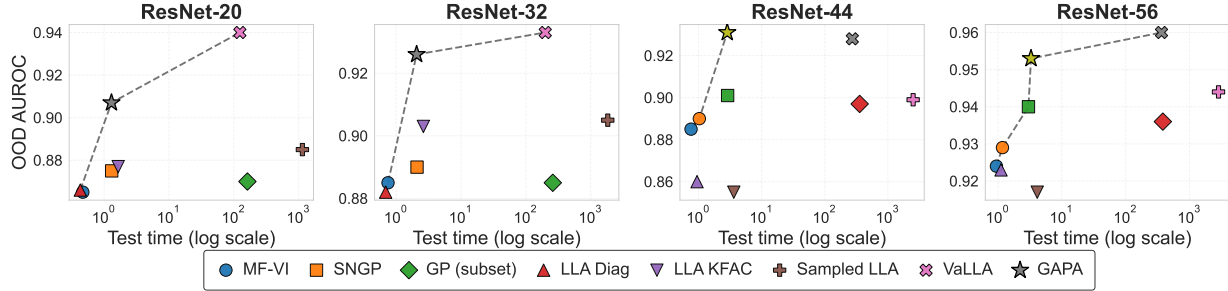


Figure 4. OOD detection vs inference cost on CIFAR-10. OOD AUROC is plotted against test-time inference cost (log scale) for ResNet backbones. Dashed lines indicate Pareto frontiers (higher OOD, lower cost). GAPA consistently lies on the frontier, achieving strong OOD performance at substantially lower inference cost than baselines.

provide additional ablation experiments on the inducing point selection. Uncertainty propagation rules for key LLM model components, such as self attention or RMS_{Norm} we detail in Appendix K.

As in classification, after variance propagation the output layer yields mean logits $\mu_{1:k}$ and diagonal logit variances $v_{1:k}$ from a single forward pass. Predictive uncertainty is estimated via a vectorized reparameterization step over the top- k tokens per position ($k = 512$). Specifically, we draw $S = 512$ samples $\ell^{(s)} = \mu_{1:k} + \sqrt{v_{1:k}} \odot \epsilon^{(s)}$ with $\epsilon^{(s)} \sim \mathcal{N}(0, I)$ and compute $p^{(s)} = \text{softmax}(\ell^{(s)})$, to form $\bar{p} = \frac{1}{S} \sum_{s=1}^S p^{(s)}$. This procedure introduces no additional network evaluations; sampling occurs only in logit space.

Uncertainty is then decomposed using entropy as

$$\text{TU} = H(\bar{p}), \text{AU} = \frac{1}{S} \sum_{s=1}^S H(p^{(s)}), \text{EU} = \text{TU} - \text{AU},$$

where $H(p) = -\sum_v p_v \log p_v$. This corresponds to the

mutual-information decomposition of uncertainty.

We define two datasets: ID (WikiText-103, validation data) and OOD (OpenWebText); each sequence is labeled $y \in \{0, 1\}$. We filter BOS/EOS and extra whitespaces around punctuation marks (WikiText-103) to avoid trivial cues; OpenWebText is prepared analogously. Note that OpenWebText is most likely not OOD for the pretrained LLaMA model itself; however, it is OOD relative to the employed method. The task is, given a sequence to distinguish these two classes based on the predictive distribution. For scoring, we compute EU, AU at every position and average over the sequence (the GAPA-based method is bold); AUROC is then computed against the sequence label. We include last-layer Laplace (trained on WikiText-103, training data) as additional baseline. Additionally, we include a temperature-scaling oracle that searches τ to maximize test AUROC using $-\sum_{v=1}^V \text{softmax}(\ell/\tau)_v \log \text{softmax}(\ell/\tau)_v$. This is *not* a fair baseline (it tunes on the test metric) but provides an upper bound for a global rescaling of logits.

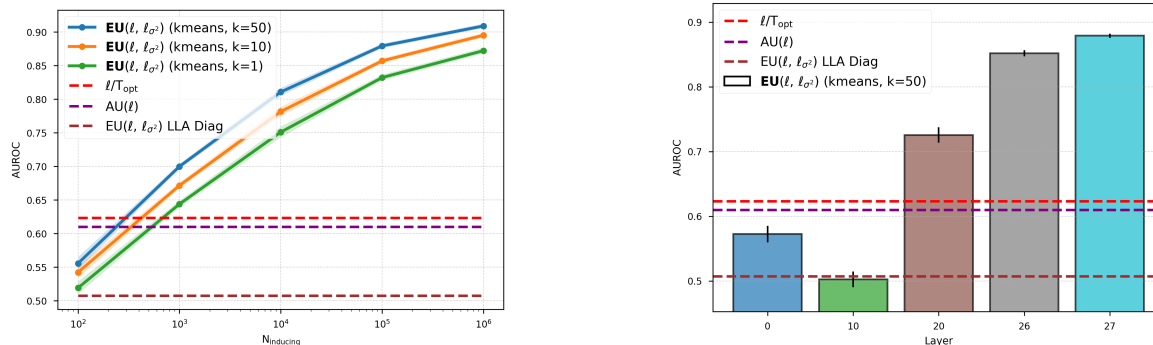


Figure 5. Left: Effect of number of inducing points N_{inducing} and k (for nearest neighbor inducing points) on OOD detection task with GAPA at layer [27]. Right: effect of layer placement of GAPA at $N_{\text{inducing}} = 10^5$. In both experiments results are averaged over 5 runs with 512 sequences each. In both panels we also show the ℓ/T_{opt} bound (green) as an upper threshold of what can be achieved by global logits scaling.

Table 5. CIFAR-10 results with ResNet-44/56 backbones. Metrics include NLL (\downarrow), OOD detection (\uparrow), and train/test runtime. Best and second-best values are highlighted in purple and teal. Results are averaged over 5 seeds; stds ($< 10^{-3}$) are omitted. Times are in seconds ($K = 10^3$). See Table 6 for additional ResNet experiments.

Model	ResNet-44				ResNet-56			
	Metrics		Time (s)		Metrics		Time (s)	
	NLL	OOD	Train	Test	NLL	OOD	Train	Test
MAP	0.275	0.885	–	0.761	0.252	0.924	–	0.949
MF-VI	0.206	0.890	1.63	1.03	0.188	0.929	1.97	1.18
SNGP	0.242	0.901	35.0	2.89	0.229	0.940	43.5	3.01
GP (subset)	0.424	0.897	8.25K	357	0.403	0.936	8.42K	382
LLA Diag	0.218	0.860	40.4	0.947	0.195	0.923	40.67	1.12
LLA KFAC	0.213	0.855	63.1	3.62	0.193	0.917	71.3	4.13
LLA*	0.237	0.895	4.98K	0.962	0.213	0.934	5.55K	1.16
LLA* KFAC	0.232	0.894	58.0	1.97	0.202	0.933	62.2	2.18
ELLA	0.204	0.885	1.12K	78.3	0.187	0.924	1.13K	91.0
Sampled LLA	0.200	0.899	11.0K	2.51K	0.185	0.944	14.6K	2.84K
VaLLA 200	0.201	0.928	16.7K	272.9	0.188	0.960	26.3K	363.8
GAPA (ours)	0.230	0.931	8.03	2.85	0.230	0.953	10.29	3.30

Fig. 5 (left) shows that GAPA-based EU surpasses the oracle logit-temperature bound once $N_{\text{inducing}} \gtrsim 10^3$, indicating that activation-space epistemics capture distributional shift not recoverable by any global rescaling of logits. Using higher number of local inducing points ($k = 50$) improves performance. Last-layer linear Laplace does not perform better than chance, we found the Fisher-matrix estimation to become close to 0. The results in Figure 5 (right) indicate that later layers improve performance with a noticeable drop in performance in the middle of the network.

4. Related Work

Uncertainty quantification methods for deep networks differ primarily in *where* uncertainty is placed and the resulting test-time cost. Since we target *frozen pretrained backbones* with *single-pass* inference, we focus on *post-hoc Bayesian*

baselines, and defer a broader discussion (sampling-based, feature-based, calibration, and activation-space training methods) to Appendix N. Laplace approximations place a Gaussian posterior over weights via a local quadratic approximation of the log posterior (MacKay, 1992; Ritter et al., 2018); last-layer variants Bayesianize only the head while keeping the feature extractor frozen, making them a standard post-hoc baseline. In contrast, GAPA places uncertainty in *activation space* and uses the original nonlinearity as the GP prior mean, preserving the frozen network’s point predictions by construction while enabling deterministic single-pass uncertainty estimation.

5. Conclusion

We introduced *GAPA*, a post-hoc uncertainty quantification method that places Bayesian modeling in *activation space* rather than weight space. By using the original nonlinearity as the GP prior mean, GAPA preserves frozen model predictions exactly while providing principled epistemic uncertainty. Designed for modern deployment constraints, GAPA employs a scalable inducing-point approximation with local KNN conditioning, yielding $O(\log M)$ inference and deterministic single-pass uncertainty estimation without sampling, retraining, or backpropagation. Across regression, classification, segmentation, and language modeling, GAPA matches or outperforms Laplace-family methods in calibration and OOD detection while achieving favorable Pareto trade-offs between uncertainty quality and inference cost, and scales to settings where last-layer methods become prohibitive (e.g., large-vocabulary language models). GAPA’s primary limitation is the memory cost of storing inducing activations. Future work includes compressed or hierarchical indexing schemes and extending beyond diagonal covariances to capture structured inter-neuron dependencies while preserving scalability.

Impact Statement

This work proposes a scalable, post-hoc method for uncertainty quantification in pretrained neural networks. The contribution is methodological in nature and is intended to improve the reliability and interpretability of model predictions. We do not foresee significant negative societal or ethical impacts beyond those commonly associated with the deployment of machine learning systems.

References

- Moloud Abdar, Farhad Pourpanah, Sadiq Hussain, Dana Rezazadegan, Li Liu, Mohammad Ghavamzadeh, Paul Fieguth, Xiaochun Cao, Abbas Khosravi, U Rajendra Acharya, et al. A review of uncertainty quantification in deep learning: Techniques, applications and challenges. *Information fusion*, 76:243–297, 2021.
- Guillaume Alain and Yoshua Bengio. Understanding intermediate layers using linear classifier probes. *arXiv preprint arXiv:1610.01644*, 2016.
- Richard Bergna, Sergio Calvo-Ordóñez, Felix L Opolka, Pietro Liò, and Jose Miguel Hernandez-Lobato. Uncertainty modeling in graph neural networks via stochastic differential equations. *arXiv preprint arXiv:2408.16115*, 2024.
- Charles Blundell, Julien Cornebise, Koray Kavukcuoglu, and Daan Wierstra. Weight uncertainty in neural network. In *International conference on machine learning*, pages 1613–1622. PMLR, 2015.
- Erik Daxberger, Agustinus Kristiadi, Alexander Immer, Runa Eschenhagen, Matthias Bauer, and Philipp Hennig. Laplace redux—effortless bayesian deep learning. *Advances in neural information processing systems*, 34:20089–20103, 2021.
- Zhijie Deng, Feng Zhou, and Jun Zhu. Accelerated linearized Laplace approximation for Bayesian deep learning. *Advances in Neural Information Processing Systems*, 35:2695–2708, 2022.
- Matthijs Douze, Alexandr Guzhva, Chengqi Deng, Jeff Johnson, Gergely Szilvassy, Pierre-Emmanuel Mazaré, Maria Lomeli, Lucas Hosseini, and Hervé Jégou. The faiss library. *IEEE Transactions on Big Data*, 2025.
- Yarin Gal and Zoubin Ghahramani. Dropout as a bayesian approximation: Representing model uncertainty in deep learning. In *international conference on machine learning*, pages 1050–1059. PMLR, 2016.
- Tilmann Gneiting and Adrian E Raftery. Strictly proper scoring rules, prediction, and estimation. *Journal of the American statistical Association*, 102(477):359–378, 2007.
- Robert B Gramacy and Daniel W Apley. Local Gaussian process approximation for large computer experiments. *Journal of Computational and Graphical Statistics*, 24(2):561–578, 2015.
- Chuan Guo, Geoff Pleiss, Yu Sun, and Kilian Q Weinberger. On calibration of modern neural networks. In *International conference on machine learning*, pages 1321–1330. PMLR, 2017.
- James Harrison, John Willes, and Jasper Snoek. Variational Bayesian last layers. *arXiv preprint arXiv:2404.11599*, 2024.
- Kaiming He, Xiangyu Zhang, Shaoqing Ren, and Jian Sun. Deep residual learning for image recognition. In *Proceedings of the IEEE conference on computer vision and pattern recognition*, pages 770–778, 2016.
- James Hensman, Nicolo Fusi, and Neil D Lawrence. Gaussian processes for big data. *arXiv preprint arXiv:1309.6835*, 2013.
- Neil Houlsby, Ferenc Huszár, Zoubin Ghahramani, and Máté Lengyel. Bayesian active learning for classification and preference learning. *arXiv preprint arXiv:1112.5745*, 2011.
- Arthur Jacot, Franck Gabriel, and Clément Hongler. Neural tangent kernel: Convergence and generalization in neural networks. *Advances in neural information processing systems*, 31, 2018.
- Balaji Lakshminarayanan, Alexander Pritzel, and Charles Blundell. Simple and scalable predictive uncertainty estimation using deep ensembles. *Advances in neural information processing systems*, 30, 2017.
- Yann LeCun, Léon Bottou, Yoshua Bengio, and Patrick Haffner. Gradient-based learning applied to document recognition. *Proceedings of the IEEE*, 86(11):2278–2324, 2002.
- Jaehoon Lee, Yasaman Bahri, Roman Novak, Samuel S Schoenholz, Jeffrey Pennington, and Jascha Sohl-Dickstein. Deep neural networks as Gaussian processes. *arXiv preprint arXiv:1711.00165*, 2017.
- Jeremiah Liu, Zi Lin, Shreyas Padhy, Dustin Tran, Tania Bedrax Weiss, and Balaji Lakshminarayanan. Simple and principled uncertainty estimation with deterministic deep learning via distance awareness. *Advances in neural information processing systems*, 33:7498–7512, 2020.
- David JC MacKay. A practical Bayesian framework for backpropagation networks. *Neural computation*, 4(3):448–472, 1992.
- Wesley J Maddox, Pavel Izmailov, Timur Garipov, Dmitry P Vetrov, and Andrew Gordon Wilson. A simple baseline for bayesian uncertainty in deep learning. *Advances in neural information processing systems*, 32, 2019.
- Andrew McHutchon and Carl Rasmussen. Gaussian process training with input noise. *Advances in neural information processing systems*, 24, 2011.
- Jishnu Mukhoti, Andreas Kirsch, Joost Van Amersfoort, Philip HS Torr, and Yarin Gal. Deep deterministic uncertainty: A new simple baseline. In *Proceedings of the IEEE/CVF Conference on Computer Vision and Pattern Recognition*, pages 24384–24394, 2023.
- Luis A Ortega, Simón Rodríguez Santana, and Daniel Hernández-Lobato. Variational linearized Laplace approximation for Bayesian deep learning. *arXiv preprint arXiv:2302.12565*, 2023.
- Omkar M Parkhi, Andrea Vedaldi, Andrew Zisserman, and CV Jawahar. Cats and dogs. In *2012 IEEE conference on computer vision and pattern recognition*, pages 3498–3505. IEEE, 2012.
- Hippolyt Ritter, Aleksandar Botev, and David Barber. A scalable laplace approximation for neural networks. In *6th international conference on learning representations, ICLR 2018-conference track proceedings*, volume 6. International Conference on Representation Learning, 2018.

Olaf Ronneberger, Philipp Fischer, and Thomas Brox. U-net: Convolutional networks for biomedical image segmentation. In *Medical image computing and computer-assisted intervention—MICCAI 2015: 18th international conference, Munich, Germany, October 5-9, 2015, proceedings, part III 18*, pages 234–241. Springer, 2015.

Hugh Salimbeni and Marc Deisenroth. Doubly stochastic variational inference for deep Gaussian processes. *Advances in neural information processing systems*, 30, 2017.

Michalis Titsias. Variational learning of inducing variables in sparse Gaussian processes. In *Artificial intelligence and statistics*, pages 567–574. PMLR, 2009.

Christopher Williams and Matthias Seeger. Using the nyström method to speed up kernel machines. *Advances in neural information processing systems*, 13, 2000.

Han Xiao, Kashif Rasul, and Roland Vollgraf. Fashion-mnist: a novel image dataset for benchmarking machine learning algorithms. *arXiv preprint arXiv:1708.07747*, 2017.

Appendix Table of Contents

Appendix A–C: theory; D–G: additional experiments; H–L: implementation details; M–N: supplementary results.

Contents

A	Conservativeness of Subset GP Conditioning	13
B	Variational Inducing-Point Interpretation and Zero-Noise Limit	13
C	Derivation for Stacking GAPA Layers	14
D	ResNets Pretrained Neural Networks	15
E	Image Segmentation	17
F	LLaMA-3.2 Additional Results	18
G	GAPA Hyperparameters	18
	G.1 GAPA Empirical Hyperparameters	18
	G.2 Regression Training Details	19
H	Nearest-Neighbour Retrieval with <code>Faiss</code>	19
	H.1 Index construction	19
	H.2 Query procedure	19
	H.3 Complexity	20
I	Laplace-Bridge Approximation for Classification	20
J	Metrics	20
	J.1 Regression Metrics	20
	J.2 Classification Metrics	20
K	Variance Propagation in Transformer Architectures	21
	K.1 Attention	21
	K.2 RMSNorm	21
	K.3 Softmax	23
L	Tables with Standard Deviations	24
	L.1 Regression	24
	L.2 Feedforward Neural Network Classification	24
	L.3 ResNet	24

M Ablation Studies	24
M.1 Where to put GAPA	24
M.2 Number of inducing inputs	24
M.3 Inducing point selection: KMeans vs. farthest-point sampling	25
M.4 Random vs Furthers Point Sampling	25
M.5 KNN Sweep: $K = 1$ to 500	26
N Extended Related Work	27

A. Conservativeness of Subset GP Conditioning

These sections provide theoretical justification for the approximations used in GAPA. We formally justify the claim made in Section 4.3 that conditioning the GP posterior on a subset of inducing inputs yields a conservative estimate of epistemic uncertainty.

Lemma 1 (Conservative uncertainty under subset conditioning). *Consider a Gaussian process prior with fixed kernel hyperparameters and Gaussian observation noise. Let \tilde{Z} denote a set of inducing inputs and let $\tilde{Z}_k \subset \tilde{Z}$ be any subset. Then, for any test input z^* , the posterior variance satisfies*

$$\text{Var}(f(z^*) | \tilde{Z}) \leq \text{Var}(f(z^*) | \tilde{Z}_k).$$

That is, conditioning on a subset of inducing inputs cannot reduce posterior variance relative to conditioning on the full inducing set.

Proof. Let $A = \tilde{Z}_k$ and $B = \tilde{Z} \setminus \tilde{Z}_k$. Under the GP prior with Gaussian observation noise, the random variables

$$(f(z^*), y_A, y_B)$$

are jointly Gaussian. The conditional covariance identity for jointly Gaussian variables gives

$$\text{Var}(f(z^*) | y_A) - \text{Var}(f(z^*) | y_A, y_B) = K_{*B|A} (K_{BB|A} + \sigma_n^2 I)^{-1} K_{B*|A},$$

where $K_{BB|A}$ and $K_{*B|A}$ denote conditional covariance matrices obtained via the Schur complement.

Since $K_{BB|A} + \sigma_n^2 I$ is positive definite, the right-hand side is positive semidefinite. Therefore,

$$\text{Var}(f(z^*) | y_A, y_B) \leq \text{Var}(f(z^*) | y_A),$$

which establishes the result. \square

This result implies that the local k -nearest-neighbour conditioning strategy used in GAPA yields a conservative approximation of epistemic uncertainty: posterior variance may be inflated due to discarded conditi

B. Variational Inducing-Point Interpretation and Zero-Noise Limit

In this appendix, we show that the inducing-point construction used in GAPA admits a variational interpretation in the sense of Titsias (Titsias, 2009), and that in the limit of vanishing observation noise the resulting posterior covariance reduces to the standard inducing-point conditional covariance.

Setup. Consider a scalar Gaussian process

$$f(\cdot) \sim \mathcal{GP}(m(\cdot), k(\cdot, \cdot)),$$

and a set of inducing inputs

$$\mathbf{Z} = \{z_m\}_{m=1}^M, \quad \mathbf{u} = f(\mathbf{Z}) \in \mathbb{R}^M.$$

Let \mathbf{z}^* denote a test input.

In GAPA, we condition the GP on noiseless pseudo-observations

$$\tilde{\mathbf{Y}} = m(\mathbf{Z}),$$

corresponding to evaluating the prior mean function at the inducing inputs. For numerical stability, we introduce an auxiliary Gaussian noise term σ_n^2 , which will be taken to zero.

Exact GP conditional. Conditioning a GP on noisy observations $\tilde{\mathbf{Y}}$ at inputs \mathbf{Z} yields the posterior covariance

$$\text{Var}(f(\mathbf{z}^*) | \tilde{\mathbf{Y}}) = k(\mathbf{z}^*, \mathbf{z}^*) - k(\mathbf{z}^*, \mathbf{Z}) (K_{\mathbf{Z}\mathbf{Z}} + \sigma_n^2 I)^{-1} k(\mathbf{Z}, \mathbf{z}^*), \quad (8)$$

where $K_{\mathbf{Z}\mathbf{Z}}$ is the kernel matrix on the inducing inputs.

Variational inducing-point posterior. Following Titsias (Titsias, 2009), the variational posterior over the inducing variables \mathbf{u} is Gaussian,

$$q(\mathbf{u}) = \mathcal{N}(\boldsymbol{\mu}, \mathbf{A}),$$

with optimal parameters

$$\boldsymbol{\mu} = \mathbf{K}_{\mathbf{Z}\mathbf{Z}}(\mathbf{K}_{\mathbf{Z}\mathbf{Z}} + \sigma_n^{-2}\mathbf{K}_{\mathbf{Z}\mathbf{Z}})^{-1}\tilde{\mathbf{Y}}, \quad \mathbf{A} = \mathbf{K}_{\mathbf{Z}\mathbf{Z}}(\mathbf{K}_{\mathbf{Z}\mathbf{Z}} + \sigma_n^{-2}\mathbf{K}_{\mathbf{Z}\mathbf{Z}})^{-1}\mathbf{K}_{\mathbf{Z}\mathbf{Z}}.$$

The corresponding variational predictive covariance at \mathbf{z}^* is

$$\text{Var}_q(f(\mathbf{z}^*)) = k(\mathbf{z}^*, \mathbf{z}^*) - k(\mathbf{z}^*, \mathbf{Z})\mathbf{K}_{\mathbf{Z}\mathbf{Z}}^{-1}k(\mathbf{Z}, \mathbf{z}^*) + k(\mathbf{z}^*, \mathbf{Z})\mathbf{K}_{\mathbf{Z}\mathbf{Z}}^{-1}\mathbf{A}\mathbf{K}_{\mathbf{Z}\mathbf{Z}}^{-1}k(\mathbf{Z}, \mathbf{z}^*). \quad (9)$$

The final term is the *variational correction* that distinguishes the variational posterior from the exact GP conditional.

Zero-noise limit. We now consider the limit $\sigma_n^2 \rightarrow 0$. In this regime,

$$\mathbf{A} = \mathbf{K}_{\mathbf{Z}\mathbf{Z}}(\mathbf{K}_{\mathbf{Z}\mathbf{Z}} + \sigma_n^2\mathbf{I})^{-1}\mathbf{K}_{\mathbf{Z}\mathbf{Z}} \xrightarrow{\sigma_n^2 \rightarrow 0} \mathbf{K}_{\mathbf{Z}\mathbf{Z}}.$$

Substituting into Eq. (9), the variational correction term becomes

$$k(\mathbf{z}^*, \mathbf{Z})\mathbf{K}_{\mathbf{Z}\mathbf{Z}}^{-1}\mathbf{K}_{\mathbf{Z}\mathbf{Z}}\mathbf{K}_{\mathbf{Z}\mathbf{Z}}^{-1}k(\mathbf{Z}, \mathbf{z}^*) = k(\mathbf{z}^*, \mathbf{Z})\mathbf{K}_{\mathbf{Z}\mathbf{Z}}^{-1}k(\mathbf{Z}, \mathbf{z}^*),$$

which exactly cancels the negative term in Eq. (9).

Therefore, the variational predictive covariance reduces to

$$\text{Var}(f(\mathbf{z}^*)) = k(\mathbf{z}^*, \mathbf{z}^*) - k(\mathbf{z}^*, \mathbf{Z})\mathbf{K}_{\mathbf{Z}\mathbf{Z}}^{-1}k(\mathbf{Z}, \mathbf{z}^*), \quad (10)$$

which is precisely the standard inducing-point conditional covariance.

Implication for GAPA. Since GAPA conditions on noiseless pseudo-observations $\tilde{\mathbf{Y}} = \phi(\mathbf{Z})$ with a prior mean $m(\cdot) = \phi(\cdot)$, the variational correction vanishes in the zero-noise limit. Consequently, the posterior covariance used by GAPA coincides with the standard inducing-point GP conditional covariance, while preserving the deterministic backbone predictions exactly.

C. Derivation for Stacking GAPA Layers

When GAPA layers are stacked, the output of a preceding GAPA layer becomes the input to a subsequent GAPA layer. Since each GAPA module produces a Gaussian output, the input to the current layer is itself a random variable. Let

$$\mathbf{z} \sim \mathcal{N}(\boldsymbol{\mu}_z, \boldsymbol{\Sigma}_z)$$

denote the pre-activation input to the current GAPA layer, where $\boldsymbol{\Sigma}_z$ is diagonal under our approximation. We write

$$\mathbf{z} = \boldsymbol{\mu}_z + \boldsymbol{\varepsilon}, \quad \boldsymbol{\varepsilon} \sim \mathcal{N}(\mathbf{0}, \boldsymbol{\Sigma}_z).$$

We consider neuron-wise propagation. For neuron i , the scalar input z_i satisfies

$$z_i = \mu_{z,i} + \varepsilon_i, \quad \varepsilon_i \sim \mathcal{N}(0, \sigma_{z,i}^2).$$

Base epistemic variance (deterministic input). Ignoring input uncertainty, the posterior variance of neuron i under the KNN GAPA approximation is given by the standard inducing-point conditional variance restricted to the local neighborhood $\mathbf{Z}_{\ell,K}(\mu_{z,i})$:

$$\sigma_{\text{epi},i}^2(\mu_{z,i}) = k_i(\mu_{z,i}, \mu_{z,i}) - \mathbf{k}_i^\top (\mathbf{K}_i + \sigma_n^2\mathbf{I})^{-1}\mathbf{k}_i, \quad (11)$$

where $\mathbf{K}_i \in \mathbb{R}^{K \times K}$ is the kernel matrix over the K nearest inducing inputs, and $[\mathbf{k}_i]_m = k_i(\mu_{z,i}, z_m)$.

Table 6. GAPA and baseline results on CIFAR-10 with ResNet backbones. This table reports the full results (including standard deviations) corresponding to Tables 9 and 10. Best results are shown in purple and second-best in teal.

	ResNet-20					ResNet-32					ResNet-44					ResNet-56				
	ACC	NLL	OOD	Train	Test	ACC	NLL	OOD	Train	Test	ACC	NLL	OOD	Train	Test	ACC	NLL	OOD	Train	Test
MAP	92.6	0.282	0.876	–	–	93.5	0.292	0.909	–	–	94.0	0.275	0.885	–	0.761	94.4	0.252	0.924	–	0.949
MF-VI	92.7	0.231	0.865	0.74	0.47	93.5	0.222	0.885	1.19	0.75	93.9	0.206	0.890	1.63	1.03	94.4	0.188	0.929	1.97	1.18
SNGP	92.4	0.266	0.875	15.9	1.31	93.2	0.256	0.890	25.5	2.10	93.8	0.242	0.901	35.0	2.89	93.8	0.229	0.940	43.5	3.01
GP (subset)	92.6	0.555	0.870	3.75K	162	93.4	0.462	0.885	6.00K	260	93.6	0.424	0.897	8.25K	357	94.4	0.403	0.936	8.42K	382
LLA Diag	92.6	0.260	0.866	18.4	0.43	93.5	0.242	0.882	29.4	0.69	94.0	0.218	0.860	40.4	0.947	94.3	0.195	0.923	40.67	1.12
LLA KFAC	92.6	0.241	0.877	28.7	1.65	93.5	0.229	0.903	45.9	2.63	94.0	0.213	0.855	63.1	3.62	94.4	0.193	0.917	71.3	4.13
Sampled LLA	92.5	0.231	0.885	5.00K	1.14K	93.5	0.217	0.905	8.00K	1.83K	94.0	0.200	0.899	11.0K	2.51K	94.4	0.185	0.944	14.6K	2.84K
VaLLA	92.4	0.231	0.940	7.59K	124	93.2	0.212	0.933	12.2K	199	93.8	0.201	0.928	16.7K	272.9	94.2	0.188	0.960	26.3K	363.8
GAPA (ours)	92.6	0.258	0.907	3.65	1.30	93.5	0.259	0.926	5.84	2.07	94.0	0.230	0.931	8.03	2.85	94.4	0.230	0.953	10.29	3.30

Input uncertainty correction (NIGP). Because the test input is uncertain, we apply the noisy-input GP (NIGP) approximation. Linearizing the posterior mean $\mu_i(z)$ around $\mu_{z,i}$ yields an additional variance term

$$\lambda_i(\mu_{z,i}) = \sigma_{z,i}^2 \left(\left. \frac{\partial \mu_i(z)}{\partial z} \right|_{z=\mu_{z,i}} \right)^2. \quad (12)$$

By construction of GAPA, the posterior mean equals the original deterministic activation,

$$\mu_i(z) = \phi_i(z),$$

so the gradient term reduces to the derivative of the activation function, and

$$\lambda_i(\mu_{z,i}) = \sigma_{z,i}^2 (\phi'_i(\mu_{z,i}))^2.$$

Total predictive variance. Combining the epistemic variance from the local inducing-point posterior, the NIGP correction due to input uncertainty, and optional observation noise $\sigma_{y,i}^2$, the total predictive variance for neuron i is

$$\text{Var}[y_i] = \underbrace{\sigma_{\text{epi},i}^2(\mu_{z,i})}_{\text{activation-space epistemic}} + \underbrace{\sigma_{z,i}^2(\phi'_i(\mu_{z,i}))^2}_{\text{propagated input uncertainty}} + \sigma_{y,i}^2. \quad (13)$$

This expression shows that stacking GAPA layers preserves mean predictions exactly while propagating uncertainty forward in closed form, with each layer contributing additional epistemic variance and attenuating or amplifying uncertainty according to the local slope of the activation function.

D. ResNets Pretrained Neural Networks

We report supplementary experiments and visualizations omitted from the main text for space.

ResNet backbones and computational trade-offs. Table 6 reports full CIFAR-10 results for pretrained ResNet backbones, including in-distribution performance (ACC/NLL), OOD detection (AUROC), and train/test runtime. Across all depths, GAPA achieves competitive in-distribution accuracy and NLL while providing strong OOD detection. Notably, methods with the strongest OOD scores (e.g., VaLLA and sampled/GP-subset baselines) often incur substantially higher computational costs, both at test time and train time.

Figure 4 visualises the robustness–efficiency trade-off by plotting OOD AUROC against test-time inference cost (log scale). Dashed lines indicate Pareto frontiers (higher OOD, lower cost), highlighting methods that offer the best compromise between reliability and efficiency. Across backbones, GAPA lies on the Pareto frontier, achieving strong OOD AUROC while avoiding the 10^2 – 10^3 s inference costs characteristic of more computationally intensive Bayesian baselines.

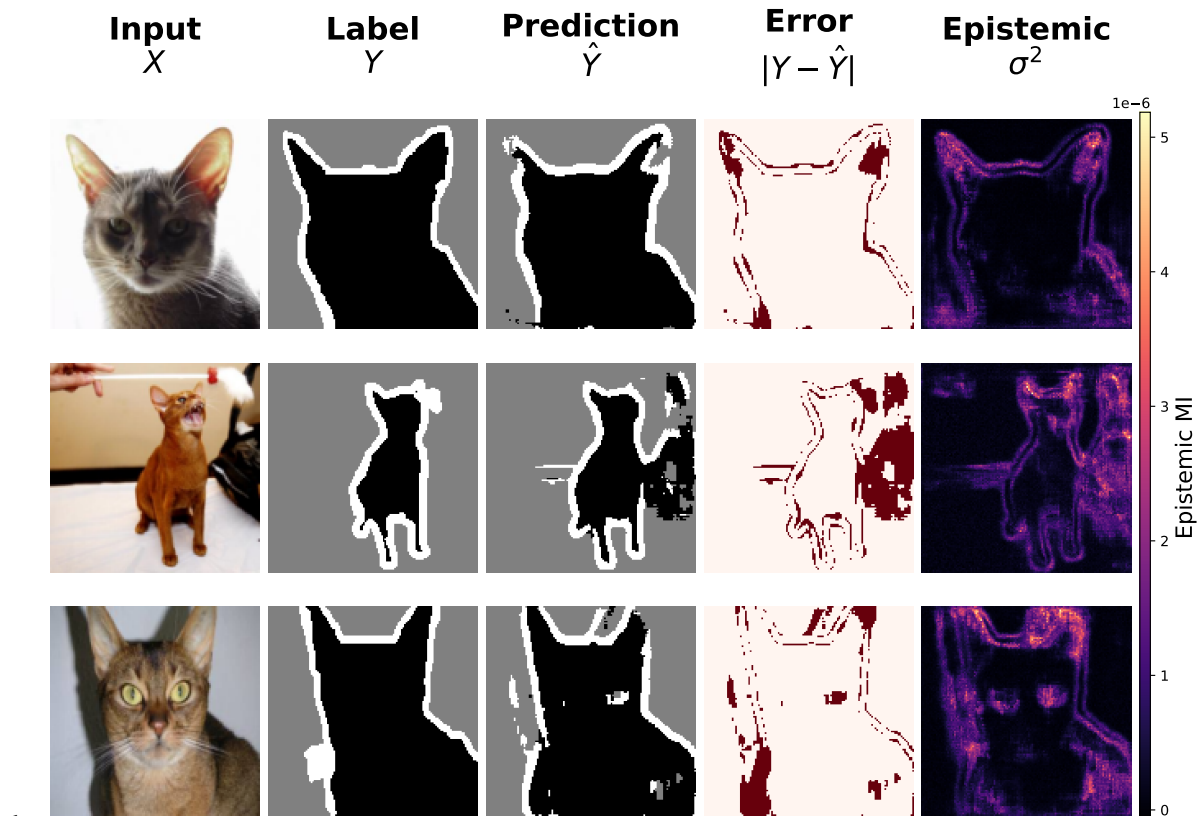


Figure 6. Qualitative segmentation results with pixel-wise error and epistemic uncertainty. **Columns:** (1) Input image X , (2) Ground-truth mask Y , (3) Predicted mask \hat{Y} , (4) Error map $|Y - \hat{Y}|$, (5) Epistemic uncertainty (mutual information). **Rows:** three representative validation examples.

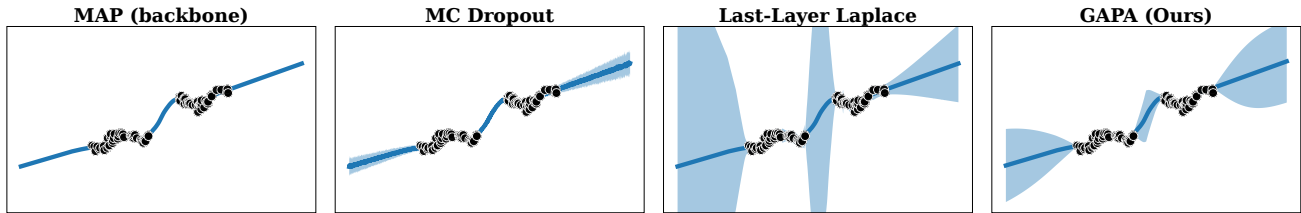


Figure 7. Regression predictions and uncertainty: (a) MAP backbone, (b) MC Dropout, (c) last-layer Laplace, (d) GAPA (ours).

E. Image Segmentation

As a proof of concept for high-dimensional outputs, we apply GAPA to a U-Net model (Ronneberger et al., 2015) pre-trained on the Oxford-IIIT Pet dataset (Parkhi et al., 2012) for a 3-class segmentation task (background, pet, outline) with input images resized to 128×128 . The U-Net architecture features an encoder path with two downsampling stages (32 and 64 channels, using double convolutions and max pooling), leading to a bottleneck with 128 channels. From this bottleneck, an embedding head comprising adaptive average pooling and a linear layer projects the features to a $d = 64$ dimensional embedding vector. Standard skip connections are used in the decoder path.

For these experiments, GAPA was applied to this $d = 64$ dimensional embedding vector at the U-Net bottleneck. This vector represents the most compressed representation in the network, and its 1D nature (after pooling and flattening). The GAPA-processed embedding (mean preserved, variance added) is then reshaped and fed into the decoder to produce the final segmentation map.

The dimensionality of the full segmentation output space (e.g., $128 \times 128 \times 3$ or $\sim 224 \times 224$ per image if referring to original dataset paper’s output size before your resize) renders methods like full Laplace approximation computationally infeasible due to memory and time constraints (e.g., matrix inversions on $\mathcal{O}(10^5)$ outputs or more). In contrast, applying GAPA at the compressed embedding stage scales efficiently. Figure 6 demonstrates that this approach not only produces accurate segmentation masks but also generates spatially localized epistemic uncertainty maps that precisely highlight regions where prediction errors occur.

F. LLaMA-3.2 Additional Results

In Figure 8 we show an additional ablation study where we compare inducing point selection using `Kmeans` or random choice. We find that random underperformed compared to `KMeans`.

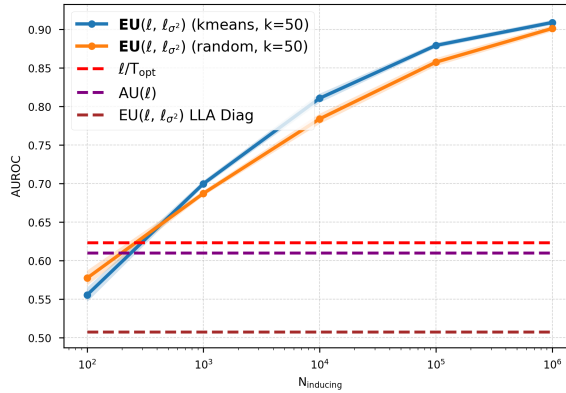


Figure 8. Effect of the number of inducing points N_{inducing} and preprocessing strategy on OOD detection task. We plot the AUC using EU (blue) with GAPA at layer [27]. Results are averaged over 5 runs with 512 sequences each. In both panels we also show the l/T_{opt} bound (green) as an upper threshold of what can be achieved by global logits scaling.

G. GAPA Hyperparameters

This section details hyperparameters, inference procedures, and architectural propagation rules.

G.1. GAPA Empirical Hyperparameters

For the **GAPA**, we deliberately avoid any gradient-based hyper-parameter optimisation. Instead, the RBF-kernel length scale ℓ_k , signal amplitude σ_k , and the set of pseudo-inputs \mathcal{Z} are fixed once from simple empirical statistics of the training data.

Length scale ℓ_k . We set every neuron’s length scale to the empirical median of all pairwise Euclidean distances between training inputs:

$$d_{ij} = \|x_i - x_j\|_2, \quad \ell_k = \text{Median}(\{d_{ij}\}).$$

In our implementation we approximate this by sampling 10^6 random pairs.

Signal variance σ_k^2 . For each hidden neuron we compute the sample standard deviation of its pre-activations over the training set:

$$\sigma_k = \text{Std}\{h_k(x_i)\}_{i=1}^N.$$

Clamped to a minimum of 10^{-6} to ensure numerical stability.

Pseudo-inputs \mathcal{Z} . With a budget of M inducing points we perform a greedy farthest-first traversal over the training inputs:

1. Select an arbitrary z_1 from the training set.
2. For $m = 2, \dots, M$, choose z_m as the training input whose minimum Euclidean distance to $\{z_1, \dots, z_{m-1}\}$ is maximal.

KMeans pseudo-inputs. As an alternative to farthest-first traversal, we also provide a KMeans-based strategy for selecting inducing points. In this variant, the pseudo-input set \mathcal{Z} consists of the M cluster centroids obtained by running KMeans on the training activations.

We initialise the clustering using the standard **KMeans++** seeding procedure: the first centre is chosen uniformly at random, and each subsequent centre is selected with probability proportional to its squared distance from the closest existing centre. This produces well-separated initial centroids and improves stability and convergence compared to random initialisation.

KMeans provides a simple, task-agnostic alternative to farthest-first traversal, and can be used interchangeably within GAPA for constructing \mathcal{Z} .

G.2. Regression Training Details

For regression, we parameterize the aleatoric variance using a small MLP head s_ψ that takes hidden representations as input:

$$\sigma_{\text{ale}}^2(\mathbf{x}) = \text{softplus}(s_\psi(\mathbf{x})) + \varepsilon$$

where $\varepsilon = 10^{-6}$ is a variance floor preventing numerical instability. The total predictive variance combines epistemic (from GAPA) and aleatoric components:

$$\sigma_{\text{tot}}^2(\mathbf{x}) = \sigma_{\text{epi}}^2(\mathbf{x}) + \sigma_{\text{ale}}^2(\mathbf{x})$$

We train only the parameters ψ by minimizing:

$$\mathcal{L}_{\text{reg}} = \frac{1}{N} \sum_{n=1}^N \left[\frac{(y_n - \mu_n)^2}{2\sigma_{\text{tot}}^2(\mathbf{x}_n)} + \frac{1}{2} \log(2\pi\sigma_{\text{tot}}^2(\mathbf{x}_n)) \right]$$

where μ_n is the fixed mean prediction from the frozen backbone. This preserves exact mean predictions while learning data-dependent noise.

H. Nearest-Neighbour Retrieval with Faiss

GAPA requires fast retrieval of the K nearest inducing activations in activation space. Given a set of inducing inputs $\mathcal{Z} = \{z_m\}_{m=1}^M \subset \mathbb{R}^d$, for each query activation z^* we compute

$$\mathcal{N}_K(z^*) = \arg \min_{\substack{S \subset \{1, \dots, M\} \\ |S|=K}} \sum_{m \in S} \|z^* - z_m\|_2.$$

A brute-force search costs $\mathcal{O}(Md)$ per query. Instead, we use `Faiss` to support efficient approximate nearest-neighbour retrieval with sublinear complexity.

H.1. Index construction

- Choice of index.** For small to moderate inducing sets we use `IndexFlatL2` (exact search). For large M , we use `IndexIVFPQ`, which partitions the space via coarse k -means clustering and stores PQ-compressed residuals (Douze et al., 2025).
- Training (optional).** Quantization-based indices (IVF, PQ) require a one-time offline training step on a representative subset of inducing activations.
- Adding vectors.** All inducing activations z_m are added once to the index; their identifiers link back to the cached kernel statistics required for GP inference.

The resulting index requires $\mathcal{O}(M)$ memory and supports K -NN queries in $\mathcal{O}(\log M)$ expected time for IVF-based indices.

H.2. Query procedure

For each test-time activation z^* :

- Query the `Faiss` index to retrieve the K nearest inducing inputs:

$$(\mathbf{d}, \mathcal{N}_K) \leftarrow \text{index.search}(z^*, K).$$

- Form the local inducing set $\mathbf{Z}_K(z^*) = \{z_m : m \in \mathcal{N}_K\}$.
- Compute the neuron-wise posterior variance using the standard inducing-point conditional restricted to this local set:

$$\text{Var}[f(z^*)] = k(z^*, z^*) - \mathbf{k}^\top (\mathbf{K}_K + \sigma_n^2 I)^{-1} \mathbf{k},$$

where \mathbf{K}_K is the $K \times K$ kernel matrix on $\mathbf{Z}_K(z^*)$ and $[\mathbf{k}]_m = k(z^*, z_m)$.

By construction, the posterior mean remains equal to the original deterministic activation, so nearest-neighbour retrieval affects only the epistemic variance.

H.3. Complexity

- *Index construction*: one-off $\mathcal{O}(Md)$ time and $\mathcal{O}(M)$ memory.
- *Query*: $\mathcal{O}(\log M)$ approximate neighbour search plus $\mathcal{O}(K^3)$ local linear algebra, with $K \ll M$ fixed.

This design keeps test-time GP inference independent of the total number of cached activations while preserving a principled, distance-aware posterior variance.

I. Laplace-Bridge Approximation for Classification

Given mean logits $\mu \in \mathbb{R}^C$ and per-class variances $\mathbf{v} \in \mathbb{R}^C$ from GAPA propagation, we compute predictive probabilities using:

$$p(y = c | \mathbf{x}) \approx \frac{\exp\left(\mu_c / \sqrt{1 + (\pi/8)v_c}\right)}{\sum_{c'=1}^C \exp\left(\mu_{c'} / \sqrt{1 + (\pi/8)v_{c'}}\right)} \quad (14)$$

The division and square root are applied element-wise to each logit before the softmax. This approximation integrates Gaussian logit uncertainty into categorical predictions without sampling, derived from the probit approximation $\Phi(x) \approx \sigma(x\sqrt{\pi/8})$ where Φ is the Gaussian CDF and σ is the sigmoid function.

J. Metrics

J.1. Regression Metrics

For evaluating performance on regression tasks (Section 3.1), we use several key metrics. First, the **Negative Log-Likelihood (NLL)** measures the quality of the predictive probability distribution. Assuming a Gaussian predictive distribution $p(y|x) = \mathcal{N}(y; \mu(x), \sigma^2(x))$, where $\mu(x)$ is the predicted mean and $\sigma^2(x)$ is the predicted variance, the NLL for a true target value y_{true} is $\frac{1}{2} \log(2\pi\sigma^2(x)) + \frac{(y_{\text{true}} - \mu(x))^2}{2\sigma^2(x)}$. Lower NLL values are better, indicating that the predictive distribution is both accurate and appropriately confident. Second, the **Continuous Ranked Probability Score (CRPS)** (Gneiting and Raftery, 2007) generalizes the Mean Absolute Error (MAE) to probabilistic forecasts. For a predictive cumulative distribution function (CDF) F and a true outcome y_{true} , it is defined as $\text{CRPS}(F, y_{\text{true}}) = \int_{-\infty}^{\infty} (F(y) - \mathbf{1}\{y \geq y_{\text{true}}\})^2 dy$, where $\mathbf{1}\{\cdot\}$ is the indicator function. For a Gaussian predictive distribution $\mathcal{N}(\mu, \sigma^2)$, a closed-form expression exists. Lower CRPS values are better, indicating a sharper and more calibrated predictive distribution. Finally, the **Centered Quantile Metric (CQM)**, as proposed by Ortega et al. (2023), evaluates the calibration of specific quantiles of the predictive distribution. It typically focuses on how well the predicted quantiles (e.g., the 5th and 95th percentiles) align with the empirical frequency of observations falling below these quantiles. A common formulation might assess the average miscalibration across symmetric quantiles, where lower CQM values generally indicate better quantile calibration.

J.2. Classification Metrics

For evaluating performance on classification tasks (Section 3.2), we use several key metrics. **Accuracy (ACC)** is the overall proportion of correctly classified samples; we note that GAPA, by design, preserves the mean predictions of the backbone network, so its ACC should match that of the original pre-trained model unless other methods being compared modify these predictions. The **Negative Log-Likelihood (NLL)**, in classification, is equivalent to the cross-entropy loss and measures the quality of the predictive probability distribution. For a given sample with true class label y_{true} (out of C classes) and where the model predicts a probability distribution $p(y|x)$ over the classes, the NLL for that sample is specifically $-\log p(y_{\text{true}}|x)$, which is the negative logarithm of the probability assigned by the model to the correct class; lower values indicate better performance. **Expected Calibration Error (ECE)** measures the discrepancy between a model’s predicted confidences and its empirical accuracies. Predictions are typically binned by their confidence scores. For each bin B_m , the accuracy $\text{acc}(B_m)$ and average confidence $\text{conf}(B_m)$ are computed. ECE is then a weighted average of the absolute difference: $\sum_{m=1}^M \frac{|B_m|}{N} |\text{acc}(B_m) - \text{conf}(B_m)|$, where N is the total number of samples; lower values indicate better calibration. For **Out-of-Distribution (OOD) Detection**, we report the Area Under the ROC curve (AUC). This evaluates the model’s ability to distinguish between in-distribution (ID) and out-of-distribution (OOD) samples based on an uncertainty score. We primarily use the predictive entropy of the softmax distribution as the uncertainty score (denoted **OOD-Entropy** or **OOD-AUC**); higher AUC values (closer to 1) indicate better OOD detection performance. We also evaluate **OOD Detection AUC with BALD (OOD-BALD)**, which is similar to the above, but the uncertainty score used for OOD detection is the

Bayesian Active Learning by Disagreement (BALD) score (Houlsby et al., 2011). BALD measures the mutual information between the model’s predictions and its parameters, often providing a better measure of epistemic uncertainty; a higher AUC indicates better OOD detection using BALD.

K. Variance Propagation in Transformer Architectures

To implement variance propagation in transformers, in addition to the classical linear layers or activation, we need three additional propagation rules: `RMSNorm`, `CausalSelfAttention` and `Softmax`.

K.1. Attention

Here, we present two variants to propagate the variance through a self-attention layer.

Given an input vector $\mathbf{x} \in \mathbb{R}^d$ with per-feature variances $\text{Var}(x_j) = v_j$, we first form the standard query/key/value projections

$$q = W^Q x, \quad k = W^K x, \quad v = W^V x,$$

with

$$\text{Var}(q_i) = \sum_{j=1}^d (W_{ij}^Q)^2 v_j, \quad \text{Var}(k_i) = \sum_{j=1}^d (W_{ij}^K)^2 v_j, \quad \text{Var}(v_i) = \sum_{j=1}^d (W_{ij}^V)^2 v_j.$$

Variant A. We treat the attention weights a_{ts} as deterministic, and propagate akin to a linear layer propagation:

$$\text{Var}(y_{t,i}) = \sum_s a_{ts}^2 \text{Var}(v_{s,i}).$$

Variant B. Let d_k be the head dimension and define the scaled logits $e_{ts} = d_k^{-1/2} q_t^\top k_s$. Under the delta method

$$\text{Var}(a_{ts}) = \frac{1}{d_k} \sum_{h=1}^{d_k} \left(q_{t,h}^2 \text{Var}(k_{s,h}) + k_{s,h}^2 \text{Var}(q_{t,h}) + \text{Var}(q_{t,h}) \text{Var}(k_{s,h}) \right).$$

After masking and applying the soft-max propagation rule of Appendix K.3 we obtain $\text{Var}(a_{ts})$. The variance of the head output is then

$$\text{Var}(y_{t,i}) = \sum_s \left[\text{Var}(a_{ts}) v_{s,i}^2 + a_{ts}^2 \text{Var}(v_{s,i}) + \text{Var}(a_{ts}) \text{Var}(v_{s,i}) \right].$$

While the second method is arguably modeling the overall variance propagation in a more sophisticated way, from a design choice perspective, the decision is not obvious: the first propagation scheme is much faster. Although we weren’t directly able to use flash attention, in theory a `FlashAttention` kernel could be modded to calculate the squared attention operation on-the-fly at no additional cost. Secondly we found that the variances can grow quickly the more layer the transformer model has because of the compounding, multiplicative effect of the variance over both the attention scores and the query, key and values. This compounding effect could be addressed with full covariance propagation, however, for transformers the embedding space is large (e.g. for LLaMA-3.2, 3B it is 4,096), making a full covariance treatment computationally intractable (and low-rank approximations either still exhibit compounding effect (if too low-rank) or again intractable). Based on these reasons in the paper use Variant A: we will assume the model knows where to look (deterministic attention weights), but is uncertain about what it sees there (value variance).

K.2. RMSNorm

Let $\mathbf{x} \in \mathbb{R}^d$ with per-feature variances $\text{Var}(x_j) = v_j$. `RMSNorm` computes the root mean square

$$\text{RMS}(\mathbf{x}) = \sqrt{\frac{1}{d} \sum_{j=1}^d x_j^2 + \varepsilon},$$

and applies the transformation

$$y_i = \gamma_i \cdot \frac{x_i}{\text{RMS}(\mathbf{x})},$$

where γ_i are learned scale parameters and $\varepsilon > 0$ is a small constant for numerical stability.

As a first-order approximation we define the expected RMS squared as

$$s^2 = \mathbb{E}\left[\frac{1}{d} \sum_{j=1}^d x_j^2\right] + \varepsilon.$$

Using the identity $\mathbb{E}[x_j^2] = \text{Var}(x_j) + \mathbb{E}[x_j]^2$, we can rewrite this as

$$\begin{aligned} s^2 &= \frac{1}{d} \sum_{j=1}^d \mathbb{E}[x_j^2] + \varepsilon \\ &= \frac{1}{d} \sum_{j=1}^d (v_j + \mathbb{E}[x_j]^2) + \varepsilon. \end{aligned}$$

Under this approximation, we treat s^2 as deterministic and propagate variance as

$$\text{Var}(y_i) \approx \frac{\gamma_i^2}{s^2} v_i.$$

The following PyTorch implementation realizes the simplified scheme:

```

1 class RMSNormVar(torch.nn.Module):
2     def __init__(self, dim: int, eps: float = 1e-6):
3         super().__init__()
4         self.eps = eps
5         self.weight = nn.Parameter(torch.ones(dim))
6
7     def _norm(self, x):
8         return x * torch.rsqrt(x.pow(2).mean(-1, keepdim=True) + self.eps)
9
10    def forward(self, input_mean, input_var):
11        """
12        Args:
13            input_mean (torch.Tensor): Input means, shape [batch_size, ..., feature_dim]
14            input_var (torch.Tensor): Input variances, shape same as input_mean
15
16        Returns:
17            tuple: (output_mean, output_var)
18        """
19
20        output_mean = self._norm(input_mean) * self.weight
21
22        # Compute expected rms squared
23        expected_rms_squared = (
24            input_mean.pow(2).mean(dim=-1, keepdim=True)
25            + input_var.mean(dim=-1, keepdim=True)
26            + self.eps
27        )
28
29        # Compute output variances

```

```

30     output_var = input_var / expected_rms_squared * self.weight.pow(2)
31
32     return output_mean, output_var
    
```

K.3. Softmax

For softmax we follow the Delta method approach. We note that this method is only used for the second variant of SelfAttention, whereas in this paper we use the first variant.

Let $\mathbf{x} \in \mathbb{R}^K$ with per-feature variances $\text{Var}(x_i) = v_i$. The softmax output is

$$s_k = \frac{e^{x_k}}{\sum_{j=1}^K e^{x_j}}.$$

The Jacobian of the softmax for fixed k is

$$\frac{\partial s_k}{\partial x_i} = s_k (\delta_{ik} - s_i).$$

Applying the Delta method with $\Sigma_{\mathbf{x}} = \text{diag}(v_1, \dots, v_K)$ gives

$$\text{Var}(s_k) = \sum_{i=1}^K \left(s_k (\delta_{ik} - s_i) \right)^2 v_i.$$

If we split out the $i = k$ term and the $i \neq k$ terms, this expands to

$$\begin{aligned} \text{Var}(s_k) &= s_k^2 (1 - s_k)^2 v_k + \sum_{i \neq k} s_k^2 s_i^2 v_i \\ &= s_k^2 \left[(1 - s_k)^2 v_k + \sum_{i \neq k} s_i^2 v_i \right]. \end{aligned}$$

```

1 def softmax_var(y_mean, x_var, axis=-1):
2     y = y_mean.transpose(axis, -1)
3     v = x_var.transpose(axis, -1)
4     W = y.pow(2) * v
5     S = W.sum(dim=-1, keepdim=True)
6     sum_excluding_k = S - W
7     diag_term = (1 - y).pow(2) * v
8     var_last = y.pow(2) * (diag_term + sum_excluding_k)
9     return var_last.transpose(-1, axis)
    
```

Table 7. Results on regression datasets with standard deviations (in $\times 10^{-3}$ units). Best values are in purple, and second-best in teal. An asterisk (*) indicates a last-layer LLA variant. Results are averages over 5 random seeds. This is the full version of Table 3 with stds included.

Model	Airline			Year			Taxi		
	NLL	CRPS	CQM	NLL	CRPS	CQM	NLL	CRPS	CQM
MAP (backbone)	5.121 (± 0.5)	18.695 (± 0.6)	0.148 (± 0.4)	3.673 (± 0.4)	5.023 (± 0.5)	0.134 (± 0.3)	3.775 (± 0.5)	3.755 (± 0.4)	0.211 (± 0.4)
LLA Diag	5.125 (± 0.4)	18.648 (± 0.5)	0.143 (± 0.3)	3.647 (± 0.3)	4.917 (± 0.4)	0.088 (± 0.2)	3.722 (± 0.4)	3.990 (± 0.5)	0.257 (± 0.3)
LLA KFAC	5.127 (± 0.3)	18.631 (± 0.4)	0.142 (± 0.3)	3.648 (± 0.3)	4.915 (± 0.4)	0.086 (± 0.2)	3.706 (± 0.3)	3.986 (± 0.4)	0.256 (± 0.3)
LLA*	5.127 (± 0.4)	18.631 (± 0.5)	0.141 (± 0.3)	3.648 (± 0.3)	4.915 (± 0.4)	0.086 (± 0.2)	3.726 (± 0.4)	3.985 (± 0.5)	0.256 (± 0.3)
LLA* KFAC	5.127 (± 0.3)	18.631 (± 0.4)	0.141 (± 0.3)	3.648 (± 0.3)	4.914 (± 0.4)	0.086 (± 0.2)	3.726 (± 0.4)	3.985 (± 0.4)	0.256 (± 0.3)
ELLA	5.388 (± 0.6)	21.671 (± 0.7)	0.413 (± 0.5)	4.020 (± 0.5)	6.049 (± 0.6)	0.424 (± 0.4)	3.885 (± 0.5)	3.680 (± 0.4)	0.219 (± 0.4)
VaLLA 100	4.963 (± 0.3)	18.814 (± 0.5)	0.099 (± 0.2)	3.515 (± 0.3)	5.004 (± 0.5)	0.047 (± 0.2)	3.235 (± 0.3)	3.999 (± 0.4)	0.149 (± 0.2)
VaLLA 200	4.965 (± 0.3)	18.788 (± 0.4)	0.098 (± 0.2)	3.485 (± 0.3)	4.970 (± 0.4)	0.041 (± 0.2)	3.232 (± 0.3)	3.979 (± 0.4)	0.142 (± 0.2)
Dropout	5.102 (± 0.5)	19.066 (± 0.6)	0.938 (± 0.5)	3.689 (± 0.5)	5.128 (± 0.5)	0.939 (± 0.4)	3.849 (± 0.6)	4.592 (± 0.6)	0.951 (± 0.5)
Ensemble	5.053 (± 0.4)	18.205 (± 0.5)	0.933 (± 0.4)	3.639 (± 0.4)	4.833 (± 0.5)	0.938 (± 0.4)	3.631 (± 0.5)	3.384 (± 0.5)	0.961 (± 0.4)
GAPA (ours)	4.946 (± 0.3)	18.068 (± 0.4)	0.103 (± 0.3)	3.470 (± 0.3)	4.663 (± 0.4)	0.014 (± 0.2)	3.112 (± 0.3)	4.035 (± 0.4)	0.104 (± 0.2)

Table 8. Results on classification datasets with standard deviations (in $\times 10^{-3}$ units). Best values are in purple, second-best in teal. Values are averages over 5 random seeds; consistent with $< 10^{-3}$ in all cases.

Model	MNIST					FMNIST				
	ACC	NLL	ECE	OOD	BALD	ACC	NLL	ECE	OOD	BALD
MAP	0.978 (± 0.4)	0.068 (± 0.2)	0.005 (± 0.3)	0.919 (± 0.5)	0.919 (± 0.4)	0.859 (± 0.3)	0.392 (± 0.6)	0.007 (± 0.3)	0.846 (± 0.5)	0.821 (± 0.5)
LLA Diag	0.976 (± 0.5)	0.177 (± 0.5)	0.105 (± 0.6)	0.932 (± 0.6)	0.941 (± 0.5)	0.856 (± 0.4)	0.421 (± 0.5)	0.057 (± 0.4)	0.872 (± 0.5)	0.873 (± 0.6)
LLA KFAC	0.978 (± 0.4)	0.102 (± 0.4)	0.042 (± 0.4)	0.971 (± 0.3)	0.971 (± 0.4)	0.858 (± 0.4)	0.395 (± 0.5)	0.020 (± 0.3)	0.909 (± 0.4)	0.970 (± 0.5)
LLA*	0.978 (± 0.4)	0.070 (± 0.3)	0.009 (± 0.3)	0.924 (± 0.5)	0.924 (± 0.5)	0.859 (± 0.4)	0.395 (± 0.5)	0.019 (± 0.3)	0.850 (± 0.5)	0.716 (± 0.5)
LLA* KFAC	0.979 (± 0.3)	0.070 (± 0.3)	0.009 (± 0.2)	0.923 (± 0.4)	0.928 (± 0.5)	0.859 (± 0.4)	0.394 (± 0.5)	0.017 (± 0.3)	0.849 (± 0.4)	0.717 (± 0.6)
ELLA	0.978 (± 0.4)	0.068 (± 0.3)	0.005 (± 0.2)	0.919 (± 0.4)	0.912 (± 0.5)	0.859 (± 0.4)	0.392 (± 0.5)	0.007 (± 0.3)	0.846 (± 0.4)	0.765 (± 0.6)
VaLLA 100	0.978 (± 0.3)	0.068 (± 0.3)	0.005 (± 0.2)	0.919 (± 0.4)	0.934 (± 0.4)	0.865 (± 0.3)	0.382 (± 0.4)	0.019 (± 0.3)	0.925 (± 0.4)	0.963 (± 0.5)
VaLLA 200	0.978 (± 0.4)	0.068 (± 0.3)	0.005 (± 0.2)	0.919 (± 0.4)	0.934 (± 0.4)	0.867 (± 0.3)	0.378 (± 0.4)	0.020 (± 0.3)	0.937 (± 0.4)	0.970 (± 0.5)
Linear Probing	0.977 (± 0.4)	0.117 (± 0.4)	0.015 (± 0.4)	0.884 (± 0.5)	0.883 (± 0.5)	0.858 (± 0.4)	0.395 (± 0.5)	0.048 (± 0.5)	0.785 (± 0.5)	0.776 (± 0.5)
GPP	0.978 (± 0.3)	1.648 (± 0.5)	0.784 (± 0.5)	0.934 (± 0.5)	0.904 (± 0.5)	0.857 (± 0.4)	1.716 (± 0.5)	0.692 (± 0.6)	0.867 (± 0.5)	0.962 (± 0.5)
Dropout	0.978 (± 0.4)	0.072 (± 0.3)	0.009 (± 0.3)	0.923 (± 0.4)	0.944 (± 0.4)	0.858 (± 0.4)	0.393 (± 0.5)	0.009 (± 0.3)	0.850 (± 0.4)	0.911 (± 0.4)
Ensemble	0.979 (± 0.3)	0.069 (± 0.3)	0.038 (± 0.5)	0.936 (± 0.5)	0.962 (± 0.4)	0.839 (± 0.5)	0.473 (± 0.6)	0.041 (± 0.4)	0.876 (± 0.5)	0.983 (± 0.5)
GAPA (ours)	0.978 (± 0.3)	0.109 (± 0.4)	0.049 (± 0.4)	0.960 (± 0.4)	0.972 (± 0.4)	0.859 (± 0.4)	0.389 (± 0.5)	0.013 (± 0.3)	0.973 (± 0.4)	0.993 (± 0.3)

L. Tables with Standard Deviations

L.1. Regression

L.2. Feedforward Neural Network Classification

L.3. ResNet

M. Ablation Studies

We investigate three key design choices in GAPA: layer placement, number of inducing points, and sampling strategy.

M.1. Where to put GAPA

Table 11 (and Figure 9) examines GAPA placement across our 4-layer network. For MNIST, placing GAPA at layer 3 achieves the best NLL (0.068), while layer 4 or any combination including layer 4 maximizes OOD detection (0.953 AUC, 0.961 BALD). For FMNIST, similar patterns emerge: layer 3 minimizes NLL (0.309), while layer 4 dominates OOD metrics (0.973 AUC, 0.969 BALD). Interestingly, adding more GAPA layers generally degrades NLL while maintaining strong OOD performance, suggesting a trade-off between calibration and uncertainty awareness. The final layer (closest to output) appears most critical for OOD detection, while intermediate layers better preserve calibration.

M.2. Number of inducing inputs

Table 11 shows performance as M increases from 10 to 55,000. Both datasets exhibit clear saturation: MNIST plateaus around $M = 40,000$ (NLL: 0.119 \rightarrow 0.117, OOD: 0.953), while FMNIST shows similar convergence. Computational costs

Table 9. GAPA and baselines on CIFAR-10 with ResNet-20 and ResNet-32. Best in purple, second-best in teal. Results shown as mean (\pm std) over 5 runs.

	ResNet-20					ResNet-32				
	ACC	NLL	OOD	Train	Test	ACC	NLL	OOD	Train	Test
MAP	92.6 (± 0.06)	0.282 (± 0.10)	0.876 (± 0.10)	–	–	93.5 (± 0.06)	0.292 (± 0.10)	0.909 (± 0.10)	–	–
MF-VI	92.7 (± 0.12)	0.231 (± 0.15)	0.865 (± 0.12)	0.74 (± 0.04)	0.47 (± 0.02)	93.5 (± 0.11)	0.222 (± 0.15)	0.885 (± 0.12)	1.19 (± 0.06)	0.75 (± 0.04)
SNGP	92.4 (± 0.08)	0.266 (± 0.12)	0.875 (± 0.10)	15.9 (± 0.8)	1.31 (± 0.07)	93.2 (± 0.08)	0.256 (± 0.12)	0.890 (± 0.10)	25.5 (± 1.3)	2.10 (± 0.11)
LLA Diag	92.6 (± 0.08)	0.260 (± 0.12)	0.866 (± 0.10)	18.4 (± 0.9)	0.43 (± 0.02)	93.5 (± 0.07)	0.242 (± 0.12)	0.882 (± 0.10)	29.4 (± 1.5)	0.69 (± 0.03)
Sampled LLA	92.5 (± 0.09)	0.231 (± 0.14)	0.885 (± 0.12)	5.00K (± 0.25 K)	1.14K (± 0.06 K)	93.5 (± 0.08)	0.217 (± 0.14)	0.905 (± 0.12)	8.00K (± 0.40 K)	1.83K (± 0.09 K)
VaLLA	92.4 (± 0.10)	0.231 (± 0.15)	0.940 (± 0.12)	7.59K (± 0.38 K)	124 (± 6)	93.2 (± 0.09)	0.212 (± 0.15)	0.933 (± 0.12)	12.2K (± 0.61 K)	199 (± 10)
GAPA (ours)	92.6 (± 0.07)	0.258 (± 0.12)	0.907 (± 0.10)	3.65 (± 0.18)	1.30 (± 0.07)	93.5 (± 0.07)	0.259 (± 0.12)	0.926 (± 0.10)	5.84 (± 0.29)	2.07 (± 0.10)

Table 10. GAPA and baselines on CIFAR-10 with ResNet-44 and ResNet-56. Best in purple, second-best in teal. Results shown as mean (\pm std) over 5 runs.

	ResNet-44					ResNet-56				
	ACC	NLL	OOD	Train	Test	ACC	NLL	OOD	Train	Test
MAP	94.0 (± 0.05)	0.275 (± 0.10)	0.885 (± 0.10)	–	0.761 (± 0.04)	94.4 (± 0.05)	0.252 (± 0.10)	0.924 (± 0.10)	–	0.949 (± 0.05)
MF-VI	93.9 (± 0.10)	0.206 (± 0.14)	0.890 (± 0.12)	1.63 (± 0.08)	1.03 (± 0.05)	94.4 (± 0.10)	0.188 (± 0.14)	0.929 (± 0.12)	1.97 (± 0.10)	1.18 (± 0.06)
SNGP	93.8 (± 0.07)	0.242 (± 0.12)	0.901 (± 0.10)	35.0 (± 1.8)	2.89 (± 0.14)	93.8 (± 0.07)	0.229 (± 0.12)	0.940 (± 0.10)	43.5 (± 2.2)	3.01 (± 0.15)
LLA Diag	94.0 (± 0.07)	0.218 (± 0.12)	0.860 (± 0.10)	40.4 (± 2.0)	0.947 (± 0.05)	94.3 (± 0.06)	0.195 (± 0.12)	0.923 (± 0.10)	40.7 (± 2.0)	1.12 (± 0.06)
Sampled LLA	94.0 (± 0.08)	0.200 (± 0.13)	0.899 (± 0.12)	11.0K (± 0.55 K)	2.51K (± 0.13 K)	94.4 (± 0.07)	0.185 (± 0.13)	0.944 (± 0.12)	14.6K (± 0.73 K)	2.84K (± 0.14 K)
VaLLA	93.8 (± 0.09)	0.201 (± 0.14)	0.928 (± 0.12)	16.7K (± 0.84 K)	272.9 (± 14)	94.2 (± 0.08)	0.188 (± 0.14)	0.960 (± 0.12)	26.3K (± 1.32 K)	363.8 (± 18)
GAPA (ours)	94.0 (± 0.06)	0.230 (± 0.12)	0.931 (± 0.10)	8.03 (± 0.40)	2.85 (± 0.14)	94.4 (± 0.06)	0.230 (± 0.12)	0.953 (± 0.10)	10.29 (± 0.51)	3.30 (± 0.17)

scale sub-linearly due to FAISS indexing—setup time increases from 2.7s to 455s for MNIST, while inference remains tractable (7.5s \rightarrow 20s). This demonstrates GAPA’s efficiency: near-optimal uncertainty quantification is achievable with moderate M values, making the method practical for larger models.

M.3. Inducing point selection: KMeans vs. farthest-point sampling

We compare two strategies for selecting inducing points: the farthest-point sampling (FPS) method used in the main paper, and the KMeans-based option introduced in Appendix G.1. Figures 10–11 report results for MNIST and FMNIST across a range of inducing-point budgets M .

Overall, both methods exhibit similar behaviour: performance improves monotonically with M and saturates once a sufficient coverage of the activation space is achieved. KMeans, however, provides a more efficient trade-off between coverage and inducing-point count, reaching its plateau at substantially smaller M values than FPS. This makes KMeans a practical alternative when memory, storage, or index construction time is a constraint.

M.4. Random vs Furthers Point Sampling

Table 11 reveals that furthest point sampling (FPS) and random sampling exhibit different strengths. At smaller M (5K-10K), random sampling achieves better NLL and OOD detection, likely because FPS’s greedy selection may overfit to specific activation patterns. However, as M increases to 40K, FPS shows marginal improvements, suggesting its structured coverage becomes beneficial with sufficient inducing points. The convergence of both methods at large M indicates that with enough

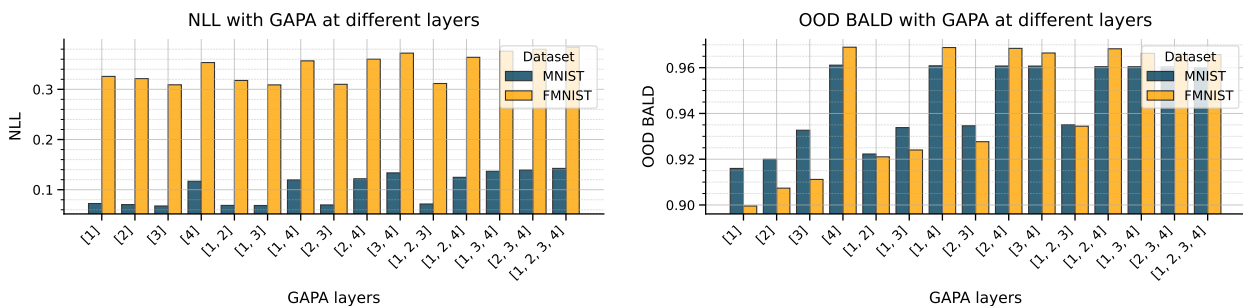

Figure 9. Comparison of metrics at different GAPA layer placements ($M = 55,000$)

Table 11. Comparison of metrics at different GAPA layer placements ($M = 55,000$). Best values are **bold**. Lower is better (\downarrow) for NLL; higher is better (\uparrow) for OOD-AUC/BALD.

GAPA layers	MNIST			FMNIST		
	NLL \downarrow	OOD-AUC \uparrow	OOD BALD \uparrow	NLL \downarrow	OOD-AUC \uparrow	OOD BALD \uparrow
[1]	0.072	0.915	0.916	0.326	0.870	0.900
[2]	0.070	0.921	0.920	0.321	0.884	0.907
[3]	0.068	0.933	0.933	0.309	0.901	0.911
[4]	0.117	0.951	0.957	0.353	0.973	0.969
[1, 2]	0.069	0.923	0.922	0.318	0.901	0.921
[1, 3]	0.069	0.934	0.934	0.309	0.912	0.924
[1, 4]	0.120	0.953	0.961	0.357	0.973	0.969
[2, 3]	0.070	0.935	0.935	0.310	0.917	0.928
[2, 4]	0.122	0.953	0.961	0.360	0.973	0.968
[3, 4]	0.134	0.953	0.961	0.372	0.973	0.966
[1, 2, 3]	0.072	0.936	0.935	0.312	0.924	0.934
[1, 2, 4]	0.125	0.953	0.960	0.364	0.973	0.968
[1, 3, 4]	0.137	0.953	0.960	0.376	0.973	0.966
[2, 3, 4]	0.139	0.953	0.960	0.380	0.973	0.966
[1, 2, 3, 4]	0.142	0.953	0.960	0.384	0.974	0.966

inducing points, the activation space is well-covered regardless of sampling strategy.

M.5. KNN Sweep: $K = 1$ to 500

To evaluate the robustness of the KNN GAPA approximation used in GAPA, we performed a comprehensive KNN sweep over $K = \{1, 2, 3, 5, 10, 20, 50, 100, 150, 200, 300, 400, 500\}$ on both MNIST and FMNIST. For each K , we recomputed the GP posterior variance using the K nearest cached activations and measured all uncertainty metrics (NLL, ECE, OOD-AUC, OOD-BALD) as well as test-time inference cost.

Across all metrics and datasets, the results reveal a strikingly consistent pattern: **all curves improve smoothly and monotonically with K** , and we observed no instability—even at $K = 1$.

Negative Log-Likelihood (NLL). NLL decreases continuously as K increases for both datasets. MNIST improves from ≈ 0.092 at $K=1$ to ≈ 0.081 at $K=500$. FMNIST improves from ≈ 0.408 at $K=1$ to ≈ 0.390 at $K=500$.

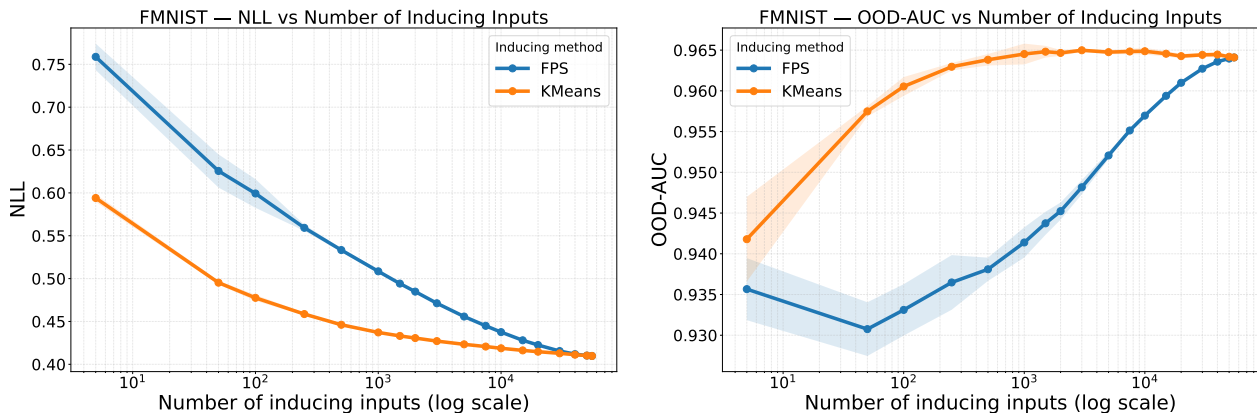
Expected Calibration Error (ECE). ECE improves monotonically for both datasets. MNIST decreases from ≈ 0.062 to ≈ 0.015 . FMNIST shows a similar smooth trend.

Expected Calibration Error (ECE). ECE improves monotonically for both datasets. MNIST decreases from ≈ 0.062 to ≈ 0.015 . FMNIST shows a similar smooth trend.

OOD-AUC. OOD detection improves slightly with K . MNIST increases from 0.950 ($K=1$) to 0.963 ($K=500$). FMNIST improves up to $K \approx 50$, then plateaus or slightly degrades for very large K due to over-smoothing.

Table 12. Metrics across different M values for MNIST and FMNIST, GAPA at the 4th layer.

M	MNIST					FMNIST				
	NLL ↓	OOD ↑	BALD ↑	set up/s ↓	inference/s ↓	NLL ↓	OOD ↑	BALD ↑	set up/s ↓	inference/s ↓
10	0.248	0.897	0.919	2.733	7.517	0.489	0.957	0.936	0.257	7.584
100	0.248	0.897	0.919	185.477	7.478	0.489	0.957	0.936	181.340	7.625
1000	0.246	0.898	0.920	184.787	7.674	0.486	0.957	0.937	183.503	7.763
5000	0.219	0.913	0.934	195.889	8.663	0.470	0.960	0.943	194.468	8.702
10000	0.181	0.933	0.950	212.990	10.119	0.442	0.964	0.952	211.333	9.873
20000	0.139	0.947	0.958	247.684	12.498	0.390	0.970	0.964	241.000	12.164
40000	0.119	0.953	0.961	301.511	16.926	0.355	0.972	0.968	301.086	16.826
55000	0.117	0.953	0.961	455.735	20.445	0.353	0.973	0.969	384.825	20.527


Figure 10. FMNIST: NLL (left) and OOD-AUC (right) for KMeans vs. FPS across M .

OOD BALD. Epistemic sensitivity improves steadily for both datasets, with consistent behaviour across the entire sweep.

Test-time cost. Test-time increases roughly linearly with K for both datasets. For MNIST, inference grows from ≈ 2.1 ms to ≈ 16 ms. FMNIST follows the same scaling pattern.

Takeaway. These experiments show:

- **1-NN is already stable and competitive**, especially for OOD detection.
- Increasing K to 20–50 provides clear gains in calibration and NLL.
- Very large K has diminishing returns and incurs high compute cost.

Overall, the full sweep confirms that the KNN GAPA approximation is **robust, stable, and effective**, and that GAPA behaves predictably across the entire KNN range.

N. Extended Related Work

Uncertainty quantification (UQ) in deep learning differs primarily in *where* uncertainty is placed (e.g., weights, outputs, or representations) and in the resulting training and test-time costs. We focus on the *post-hoc* regime for *frozen pretrained backbones*, where retraining, multiple test-time samples, or full-network second-order computation can be infeasible.

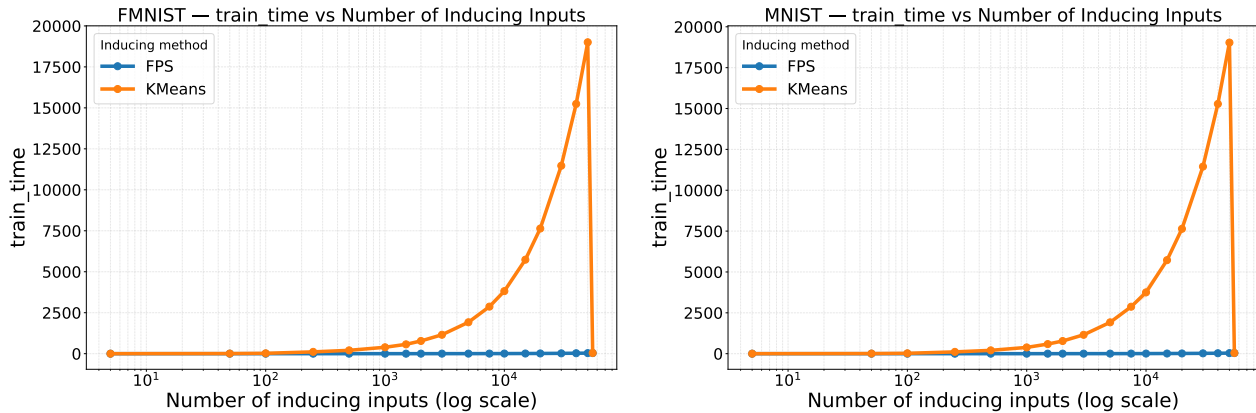


Figure 11. Setup time (FAISS indexing) for KMeans vs. FPS on FMNIST (left) and MNIST (right).

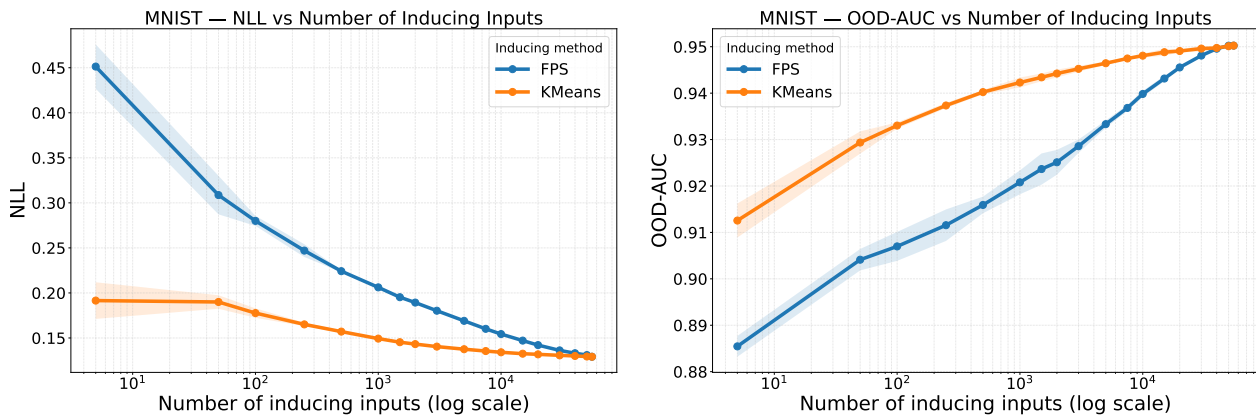


Figure 12. MNIST: NLL (left) and OOD-AUC (right) for KMeans vs. FPS across M .

Weight-space Bayesianization and Laplace. Weight-space Bayesian methods model uncertainty directly over parameters, typically requiring either approximate inference during training or posterior sampling at test time. Laplace approximations instead fit a local Gaussian posterior around a trained solution using curvature information, and recent work has revisited Laplace as a competitive and practical Bayesian deep learning baseline, including analyses of when structured approximations are necessary for scalability and fidelity (Blundell et al., 2015; MacKay, 1992; Daxberger et al., 2021; Ortega et al., 2023; Deng et al., 2022). Closely related, stochastic weight-space approximations such as SWAG provide inexpensive posterior samples from SGD trajectories and often serve as strong uncertainty baselines without changing the underlying architecture (Maddox et al., 2019).

Last-layer and single-pass post-hoc methods. A popular compromise Bayesianizes only the final layer(s) while keeping the feature extractor frozen, yielding post-hoc uncertainty at substantially reduced cost. Beyond Laplace-style last-layer treatments, deterministic variational formulations such as variational Bayesian last layers (VBLL) aim to deliver *single-pass* predictive uncertainty for frozen-backbone models (Harrison et al., 2024). These approaches are strong deployment-friendly baselines, but they concentrate Bayesian modeling at the head and do not in general propagate mean-preserving uncertainty through intermediate computations of the frozen network.

Sampling-based baselines. Deep ensembles approximate epistemic uncertainty through multiple independently trained models (Lakshminarayanan et al., 2017), while MC Dropout relies on multiple stochastic forward passes at inference (Gal and Ghahramani, 2016). These are effective but often incompatible with strict single-pass deployment constraints.

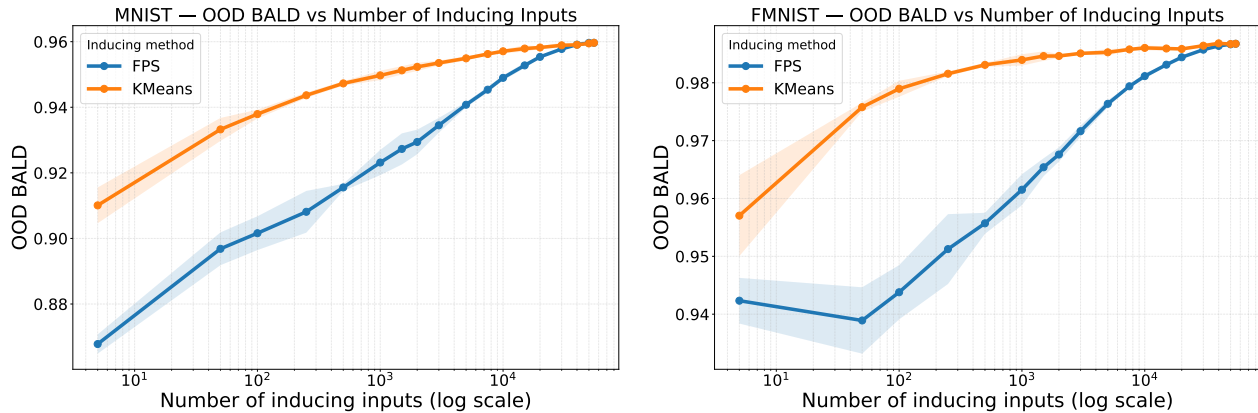


Figure 13. BALD-based OOD detection for MNIST (left) and FMNIST (right).

Table 13. Comparison of NLL and OOD BALD for FPS and three random baselines (FMNIST, gapa_index= last layer).

M	FPS NLL↓	FPS OOD↑	Rand1 NLL↓	Rand1 OOD↑	Rand2 NLL↓	Rand2 OOD↑	Rand3 NLL↓	Rand3 OOD↑
5000	0.470	0.943	0.394	0.957	0.394	0.957	0.394	0.957
10000	0.442	0.952	0.380	0.960	0.380	0.960	0.380	0.960
20000	0.390	0.964	0.369	0.964	0.369	0.964	0.369	0.964
40000	0.355	0.968	0.359	0.967	0.359	0.967	0.359	0.967

Representation-based and calibration baselines. Distance-/density-aware approaches estimate uncertainty from representations, e.g., spectral-normalized GP-style heads (SNGP) (Liu et al., 2020) or density-based uncertainty on deep features (DDU) (Mukhoti et al., 2023). Calibration-only post-processing such as temperature scaling can improve confidence calibration but does not model epistemic uncertainty (Guo et al., 2017).

Gaussian processes and function-space views. Gaussian processes (GPs) provide a classical function-space approach to uncertainty and connect naturally to infinite-width neural networks: fully-connected nets converge to an NNGP prior (Lee et al., 2017), and their infinite-width training dynamics are characterized by the NTK (Jacot et al., 2018). For scalability, GP/kernel Inference is commonly accelerated via low-rank approximations such as inducing points (Titsias, 2009) and Nyström methods (Williams and Seeger, 2000), while local GP approximations and noisy-input corrections (e.g., NIGP) provide efficient variance adjustments under locality or input uncertainty (Gramacy and Apley, 2015; McHutchon and Rasmussen, 2011). GAPA builds on these function-space ideas but applies them *inside* frozen networks by placing uncertainty in activation space, preserving the pretrained mean and enabling deterministic single-pass inference.

Summary. Overall, existing approaches trade off between (i) retraining or multi-sample inference, (ii) post-hoc last-layer approximations that concentrate uncertainty at the head, or (iii) representation-based proxies. These gaps motivate mean-preserving, post-hoc activation-space uncertainty with deterministic single-pass inference.

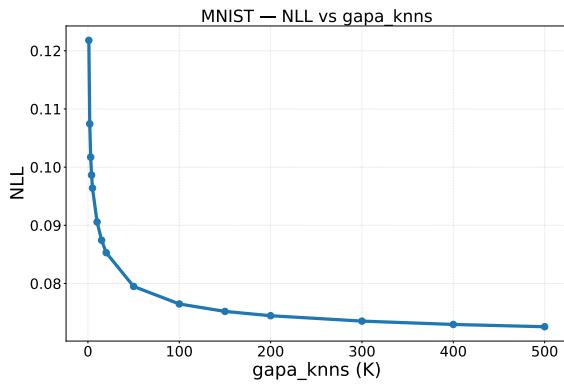


Figure 14. MNIST NLL vs. K .

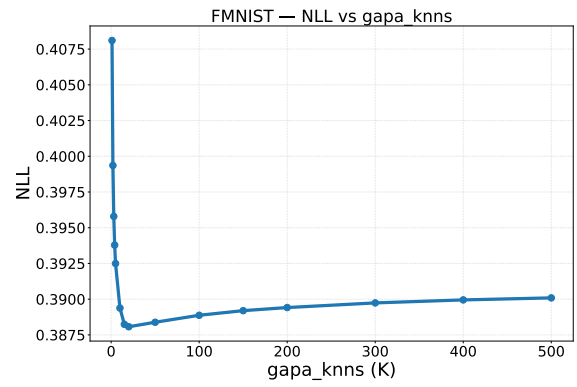


Figure 15. FMNIST NLL vs. K .

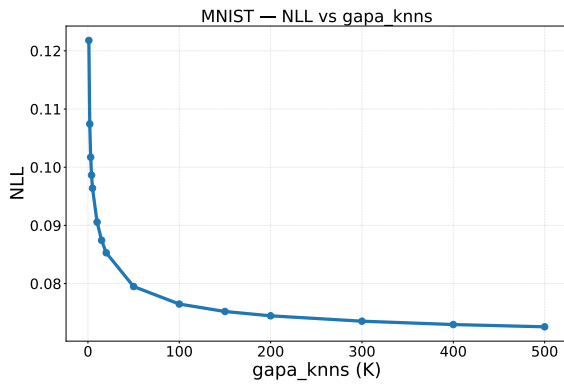


Figure 16. MNIST NLL vs. K .

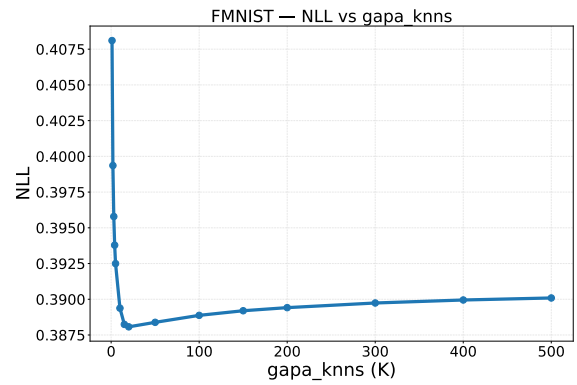


Figure 17. FMNIST NLL vs. K .

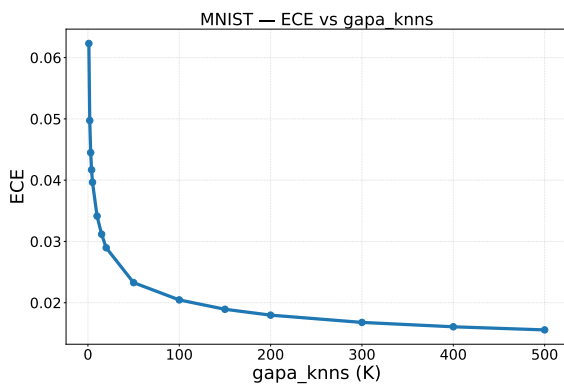


Figure 18. MNIST ECE vs. K .

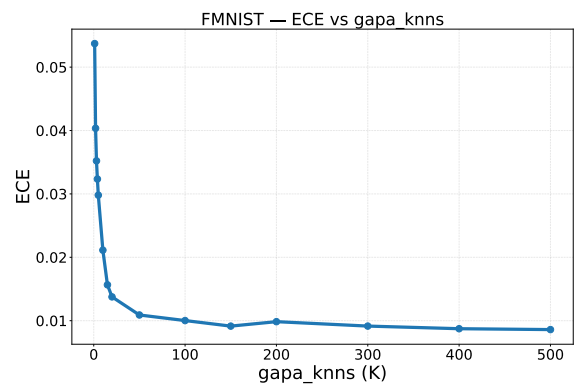


Figure 19. FMNIST ECE vs. K .

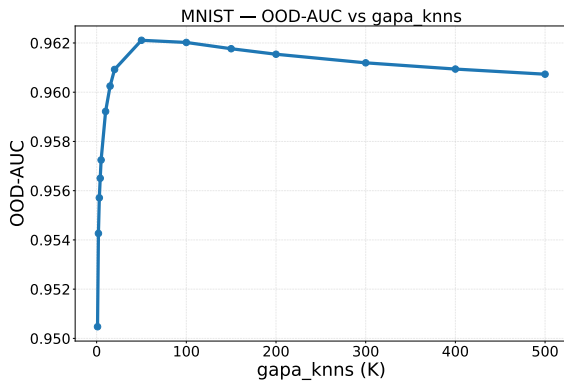


Figure 20. MNIST OOD-AUC vs. K .

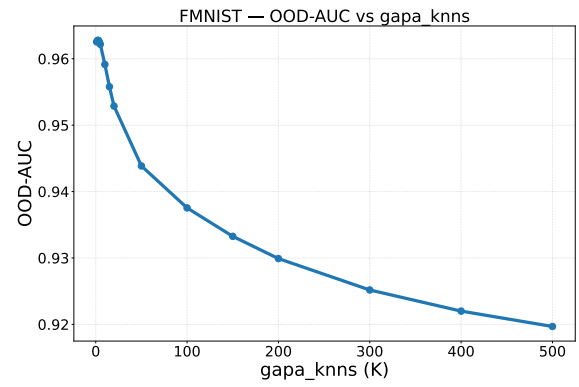


Figure 21. FMNIST OOD-AUC vs. K .

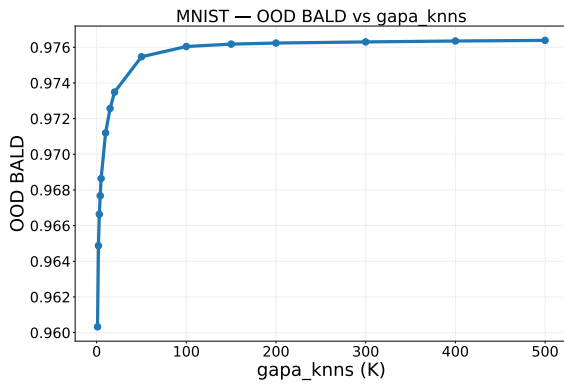


Figure 22. MNIST OOD-BALD vs. K .

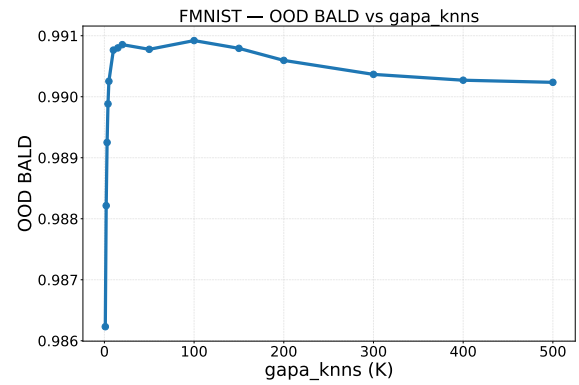


Figure 23. FMNIST OOD-BALD vs. K .

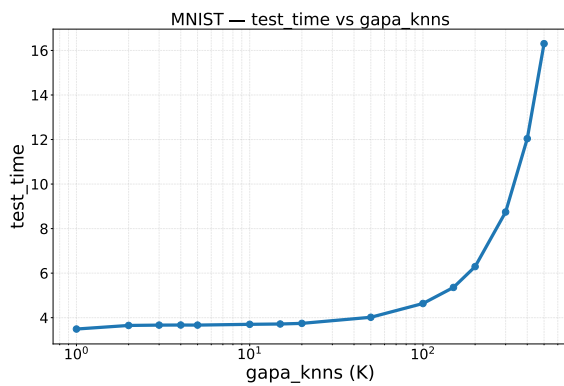


Figure 24. MNIST test time vs. K .

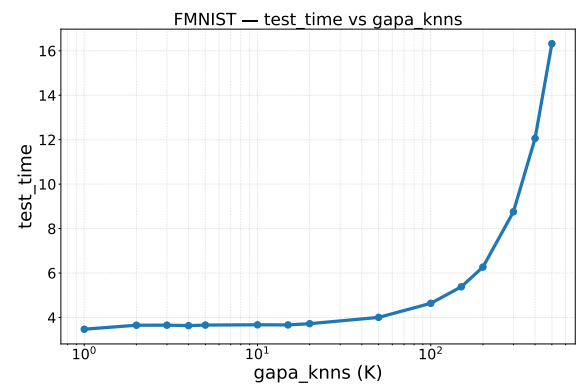


Figure 25. FMNIST test time vs. K .